Extraction and isolation

Air-dried fruit bodies of *A. blazei* (11.0 kg) were extracted three times with MeOH (4.5 l) at 25°C for 1 week and then concentrated to 3 l in vacuo. The extract was washed with *n*-hexane (3 l, 177 g) and then the MeOH layer was concentrated to a gummy mass. The latter was suspended in water (3 l) and then extracted with EtOAc (3 l) to give 70.9 g of an EtOAc-soluble fraction. The aqueous layer was extracted with 1-BuOH (3 l) to give a 1-BuOH-soluble fraction (190 g), and the remaining water layer was concentrated to furnish 1.31 kg of a water-soluble fraction.

The EtOAc-soluble fraction (70.0 g) was subjected to silica gel (1.00 kg) ($\Phi = 8$ cm, $L = 45$ cm) CC, with *n*-hexane–EtOAc [(50:1, 6 l), (20:1, 6 l), (10:1, 6 l), (5:1, 6 l), (2:1, 6 l), and (1:1, 3 l)], 6-l fractions being collected. The fourth fraction (8.4 g) was separated by silica gel (200 g) ($\Phi = 8$ cm, $L = 45$ cm) CC again with $CHCl_3$ (1.2 l) and $CHCl_3$–MeOH [(100:1, 1.2 l), (50:1, 1.2 l), (40:1, 1.2 l), (30:1, 1.2 l), (10:1, 1.2 l), (2:1, 1.2 l), and (1:1, 1.2 l)], 300-ml fractions being collected. The residue (1.18 g) in fractions 18–20 was separated by Sephadex LH-20 ($\Phi = 3$ cm, $L = 90$ cm) CC with $CHCl_3$–MeOH (1:1), 10-g fractions being collected, and the residue (20.3 mg) in fractions 21–26 was finally purified by HPLC [GL Science Inertsil Diol, $\Phi = 6$ mm, $L = 250$ mm, *n*-hexane–EtOH (19:1), 1 ml/min] to give 4.9 mg of **7** from the peak at 33 min.

The fifth fraction (10.2 g) was separated by ODS {Cosmosil 75C_{18}-OPN (Nacalai Tesque, Kyoto, Japan) [$\Phi = 50$ mm, $L = 25$ cm, linear gradient of MeOH–H_2O (3:7, 1 l) → (1:0, 1 l), fractions of 13 g being collected]} CC to give two fractions. The first fraction was purified by HPLC [Nacalai Tesque Cosmosil 5 C18-Ar-II, $\Phi = 10$ mm, $L = 250$ mm, MeOH–H_2O (1:1), 2 ml/min] to give crude **4** (29.4 mg) and 3.6 mg of **2** from the peaks at 50–66 and 69 min, respectively. The crude **4** was repeatedly purified under the same conditions to afford 2.1 mg of pure **4** from the peak at 64 min. The latter was purified by HPLC [Merck Hibar, $\Phi = 20$ mm, $L = 250$ mm, MeOH–H_2O (19:1), 0.5 ml/min] to give impure **5** (65.9 mg), **6** (26.7 mg), and **3** (44.3 mg) from the peaks at 17, 34, and 37 min, respectively. These impure compounds were separately purified by repeated HPLC under the following conditions [GL Science Inertsil Diol, $\Phi = 10$ mm, $L = 250$ mm, *n*-hexane–EtOH (199:1), 2.8 ml/min), GL Science Inertsil Diol, $\Phi = 6$ mm, $L = 250$ mm, *n*-hexane–EtOH (199:1), 1.6 ml/min and GL Science Inertsil Diol, $\Phi = 6$ mm, $L = 250$ mm, *n*-hexane–EtOH (19:1), 1.6 ml/min, respectively] to give 10.7 mg of **5**, 6.0 mg of **6**, and 5.0 mg of **3** from the peaks at 48, 20, and 39 min, respectively.

The sixth fraction (4.2 g) was separated by ODS [Nacalai Tesque Cosmosil 75C_{18}-OPN, $\Phi = 50$ mm, $L = 25$ cm, linear gradient of MeOH–H_2O (1:9, 1 l) → (1:0, 1 l), fractions of 13 g being collected]. The residue (209 mg) in fraction 91–124 was purified by HPLC [Merck Hibar, $\Phi = 20$ mm, $L = 250$ mm, MeOH–H_2O (3:2), 3 ml/min] to yield 17.7 mg of **1** from the peak at 22 min.

1-[4-(Hydroxymethyl)phenyl]hexan-1-ol (**1**)

Amorphous powder, $[\alpha]_D^{26}$ ~0.0 (*c* 1.18, $CHCl_3$). IR ν_{max} (film) cm^{-1}: 3367, 2930, 2858, 1603, 1512, 1456, 1402, 1208, 1012, 821. UV λ_{max} (MeOH) nm (log ε): 254 (3.39), 220 (3.64). ^{1}H-NMR ($CDCl_3$, 400 MHz) δ: 7.33 (4H, m, H-2, 3, 5, and 6), 4.68 (2H, s, H_2-13), 4.66 (1H, dd, $J = 8$, 6 Hz, H-7), 1.79 (1H, m, H-8a), 1.67 (1H, m, H-8b), 1.29 (6H, m, H_2-9, 10 and 11), 0.87 (3H, t, $J = 7$ Hz, H_3-12). ^{13}C-NMR ($CDCl_3$, 100 MHz): Table 1. HR-ESI–MS (positive-ion mode) *m/z*: 231.1360 $[M+Na]^+$ (Calcd for $C_{13}H_{20}O_2Na$: 231.1355).

1-[4-(Hydroxymethyl)phenyl]hexan-1-one (**2**)

Amorphous powder, IR (film) ν_{max} cm^{-1}: 3138, 2954, 2928, 2863, 1679, 1609, 1508, 1413, 1043. UV (MeOH) λ_{max} nm (log ε): 250 (4.00), 212 (3.73). ^{1}H-NMR ($CDCl_3$, 400 MHz) δ: 7.95 (2H, d, $J = 8$ Hz, H-2′ and 6′), 7.45 (2H, d, $J = 8$ Hz, H-3′ and 5′), 4.77 (2H, s, H_2-13), 2.95 (2H, t, $J = 7$ Hz, H_2-8), 1.74 (2H, m, H_2-9), 1.37 (4H, m, H_2-10 and 11), 0.91 (3H, t, $J = 7$ Hz, H_3-12). HR-ESI–MS (positive-ion mode) *m/z*: 231.1194 $[M+Na]^+$ (Calcd for $C_{13}H_{18}O_2Na$: 229.1199).

3β,5α,6α-Trihydroxyergosta-7,22-diene 6-*O*-benzoate (**3**)

Amorphous powder, $[\alpha]_D^{28}$ +29.1 (*c* 0.37, $CHCl_3$). IR ν_{max} cm^{-1}: 3,429, 2,956, 2,935, 2870, 1716, 1455, 1274, 1112, 1069, 1025, 757, 713. UV (MeOH) λ_{max} nm (log ε): 275 (3.25), 228 (3.96). ^{1}H-NMR ($CDCl_3$, 400 MHz) δ: 8.07 (2H, d, $J = 7$ Hz, H-2′ and 6′), 7.57 (1H, t, $J = 7$ Hz, H-4′), 7.45 (2H, t, $J = 7$ Hz, H-3′ and 5′), 5.54 (1H, br d, $J = 2$ Hz, H-6), 5.23 (1H, dd, $J = 15$, 7 Hz, H-23), 5.16 (1H, dd, $J = 15$, 8 Hz, H-22), 5.02 (1H, br d, $J = 2$ Hz, H-7), 4.02 (1H, dddd, $J = 11$, 11, 5, 5 Hz, H-3), 2.13 (1H, m, H-9), 2.10 (2H, m, H_2-12), 2.01 (2H, H-4a and 20), 1.88 (1H, m, H-24), 1.84 (1H, m, H-2a), 1.75 (1H, m, H-16a), 1.72 (2H, m, H-11a and 16b), 1.59 (1H, m, H-4b), 1.57 (2H, m, H-1a and 11b), 1.54 (1H, m, H-15a), 1.53 (1H, m, H-1b), 1.46 (2H, m, H-2b and 25), 1.40 (1H, m, H-15b), 1.31 (1H, m, H-14), 1.30 (1H, m, H-17), 1.08 (3H, s, H_3-19), 1.03 (3H, d, $J = 7$ Hz, H_3-21), 0.91 (3H, d, $J = 6$ Hz, H_3-28), 0.84 (3H, d, $J = 6$ Hz, H_3-27), 0.82 (3H, d, $J = 6$ Hz, H_3-26), 0.59 (3H, s, H_3-18). ^{13}C-NMR ($CDCl_3$, 100 MHz): Table 1. HR-ESI–MS (positive-ion mode) *m/z*: 557.3602 $[M+Na]^+$ (Calcd for $C_{35}H_{50}O_4Na$: 557.3601).

N-Benzoyl-L-leucine methyl ester (**4**)

Colorless crystals (MeOH), mp. 104–106°C, $[\alpha]_D^{28}$ −10.3 (*c* 0.21, EtOH). IR ν_{max} (film) cm^{-1}: 3317, 2955, 1744, 1637, 1543, 1207, 1163, 1024. UV (MeOH) λ_{max} nm (log ε): 226 (4.08). ^{1}H-NMR ($CDCl_3$, 400 MHz) δ: 7.80 (2H, dt, J = 7, 2 Hz, H-2′ and 6′), 7.51 (1H, tt, J = 7, 2 Hz, H-4′), 7.44 (1H, tt, J = 7, 2 Hz, H-3′ and 5′), 6.49 (1H, br d, J = 8 Hz, –NH–), 4.87 (1H, ddd, J = 8, 8, 5 Hz, H-1), 3.77 (3H, s $-OCH_3$), 1.79–1.65 (3H, m, H_2-2 and H-3), 1.00 (3H, d, J = 6 Hz, H_3-4), 0.98 (3H, d, J = 6 Hz, H_3-5). ^{13}C-NMR ($CDCl_3$, 100 MHz) δ: 173.7 (C-6), 167.1 (C-7′), 134.1 (C-1′), 131.7 (C-4′), 128.6 (C-3′ and 5′), 127.1 (C-2′ and 6′), 52.4 ($-OCH_3$), 51.2 (C-1), 42.1 (C-2), 25.1 (C-3), 22.8 (C-4), 22.2 (C-5). HR-ESI–MS (positive-ion mode) *m/z*: 272.1256 $[M+Na]^+$ (Calcd for $C_{14}H_{19}O_3NNa$: 272.1257).

(*R*)- (**1a**) and (*S*)-MTPA (**1b**) esters of **1**

A solution of **1** (0.9 mg) in 1 ml of dehydrated CH_2Cl_2 was reacted with (*R*)-MTPA (46 mg) in the presence of 1-ethyl-3-(3-dimethylaminopropyl)cardodiimide hydrochloride (EDC) (43 mg) and *N*,*N*-dimethyl-4-aminopyridine (4-DMAP) (22 mg), and then the mixture was occasionally stirred at 25°C for 30 min and then at 40°C for 5 min. After the addition of 1 ml of CH_2Cl_2, the solution was washed with H_2O (1 ml), 4 N HCl (1 ml), saturated aqueous $NaHCO_3$, and then brine (1 ml), successively. The organic layer was dried over Na_2SO_4 and then evaporated under reduced pressure. The residue was purified by preparative TLC [silica gel (0.25 mm thickness), being applied for 18 cm, developed with $CHCl_3$–$(CH_3)_2CO$ (20:1) for 9 cm, and then eluted with $CHCl_3$–MeOH (9:1)] to furnish ester **1a** (1.3 mg). Through a similar procedure, ester **1b** (1.2 mg) was prepared from **1** (0.9 mg) using (*S*)-MTPA (51 mg), EDC (44 mg), and 4-DMAP (24 mg). The ^{1}H-NMR spectra of **1b** and **1c** were ones of essentially the same diastereomeric mixture.

Assaying of cytotoxicity toward HepG2 cells

The cytotoxicities of the isolated compounds toward HepG2 cells were determined by means of the MTT assay. HepG2 cells were inoculated at a density of 3×10^3 cells/well in 90 μl of DMEM containing 10% FCS, supplemented with amphotericin B (Sigma Co., Ltd) (0.5 μg/ml) and kanamycin sulfate (Meiji Confectionery Co., Ltd) (100 μg/ml), on 96-well plates and then incubated at 37°C under 5% CO_2. After 24 h, 10 μl of a sample solution and etoposide in 10% DMSO was added, followed by further incubation for 72 h. The medium was removed and 100 μl of MTT (0.5 mg/ml) in DMEM was added. After 1.5 h, the medium was removed, 100 μl of DMSO was added to lyse the cells, and then the absorbance (*A*) of MTT formazan in each well was measured with a microplate reader at L_1 = 540 nm and L_2 = 620 nm. Etoposide was used as a positive control [18–20].

Activity was calculated as follows:

$$\% \text{ Inhibition} = [1 - \text{sample}(A_{L_1} - A_{L_2})/\text{control}(A_{L_1} - A_{L_2})] \times 100.$$

The results are expressed as the means with standard deviations (SD) for triplicate experiments.

Known compounds, isolated

Demethylincisterol A_3 (**5**): colorless oil, $[\alpha]_D^{26}$ +174.3 (*c* 0.81, $CHCl_3$) [9]. (22*E*,24*R*)-5α,8α-Epidioxyergosta-6,22-dien-3-β-ol (ergosterol peroxide) (**6**): colorless crystals (MeOH), mp. 180–181°C. $[\alpha]_D^{26}$ −18.3 (*c* 0.60, MeOH) [21]. (22*E*,24*R*)-3β,5α,6α-Trihydroxyergosta-7,22-diene (**7**): colorless needles (MeOH), mp. 230–232°C. $[\alpha]_D^{24}$ +11.6 (*c* 0.37, $CHCl_3$) [22].

Acknowledgments The authors thank Marukura Co., Ltd (Onojo City, Fukuoka) for supplying the fruiting bodies of *Agaricus blazei*. The authors are grateful for access to the superconducting NMR instrument at the Analytical Center of Molecular Medicine of the Graduate School of Biomedical Sciences, Hiroshima University, and an Applied Biosystem QSTAR XL system ESI (Nano Spray)–TOF–MS at the Analytical Center of Molecular Medicine and the Analysis Center of Life Science, respectively, of the Hiroshima University Faculty of Medicine.

References

1. Kimura Y, Kido T, Takaku T, Sumiyoshi M, Baba K (2004) Isolation of an anti-angiogenic substance from *Agaricus blazei* Murrill: its antitumor and antimetastatic actions. Cancer Sci 95:758–764
2. Pinheiro F, Faria RR, de Camargo JL, Spinardi-Barbisan AL, da Eira AF, Barbisan LF (2003) Chemoprevention of preneoplastic liver foci by dietary mushroom, *Agaricus blazei* Murrill in the rat. Food Chem Toxicol 2003:1543–1550
3. Itoh H, Ito H, Hibasami H (2008) Blazein of a new steroid isolated from *Agaricus blazei* Murrill (Himematsutake) induces cell death and morphological changes of apoptotic chromatin condensation in human lung cancer LU99 and stomach cancer KATO III cells. Oncol Rep 20:1359–1361
4. Ziliotto L, Pinheiro F, Barbisan LF, Rodrigues MAM (2009) Screening for in vitro and in vivo antitumor activities of the mushroom *Agaricus Blazei*. Nutr Cancer 61:245–250
5. Mukai H, Watanabe T, Ando M, Katsumata N (2006) An alternative medicine, *Agaricus blazei*, may have induced severe hepatic dysfunction in cancer patients. Jpn J Clin Oncol 36:808–810
6. Firenzuoli F, Gori L, Lombardo G (2008) The medicinal mushroom *Agaricus blazei* Murrill: review of literature and pharmacotoxicological problems. Evid Based Complement Alternat Med 5:3–15

7. Kawagishi H, Katsumi R, Sazawa T, Mizuno T, Hagiwara T, Nakamura T (1988) Cytotoxic steroids from the mushroom *Agaricus blazei*. Phytochemistry 27:2777–2779
8. Hirotani M, Sai K, Hirotani S, Yoshioka T (2002) Blazeispirols B, C, E and F, des-*A*-ergostane-type compounds, from the cultured mycelia of the fungus *Agaricus blazei*. Phytochemistry 59:571–577
9. Togashi H, Mizushima Y, Takemura M, Sugawara F, Koshino H, Esumi Y, Uzawa J, Kumagai H, Matsukage A, Yoshida S, Sakaguchi K (1998) 4-Hydroxy-17-methylincisterol, an inhibitor of DNA polymerase-α activity and the growth of human cancer cells in vitro. Biochem Pharmacol 56:583–590
10. Krzyczkowski W, Malinowska E, Suchocki P, Kleps J, Olejnik M, Herold F (2009) Isolation and quantitative determination of ergosterol peroxide in various edible mushroom species. Food Chem 113:351–355
11. Chen R, Wang Y, Yu D (1991) Chemical constituents of the spores from *Ganoderma lucidum*. Acta Botanica Sinica 33:65–68
12. Lutz C, Knochel P (1997) Highly enantioselective addition of mixed diorganozincs to aldehydes. J Org Chem 62:7895–37898
13. Li W-R, Yo Y-C, Lin Y-S (2000) Efficient one-pot formation of amides from benzyl carbamates: application to solid-phase synthesis. Tetrahedron 56:8867–8875
14. Williams MW, Young GT (1963) Amino-acids and peptides. Part XVI. Further studies of racemization during peptide synthesis. J Chem Soc 881–889. doi:10.1039/JR9630000881
15. Ciminiello P, Fattorusso E, Magno S, Mangoni A, Pansini M (1990) Incisterols, a new class of highly degraded sterols from the marine sponge *Dictyonella incise*. J Am Chem Soc 112:3505–3509
16. De Riccardis F, Spinella A, Izzo I, Giordano A, Sodano G (1995) Synthesis of (17*R*)-17-methylincisterol, a highly degraded marine steroid. Tetrahedron Lett 36:4303-4306
17. Mansoor TA, Hong J, Lee C-O, Bae S-J, Im KS, Jung JH (2005) Cytotoxic sterol derivative from a marine sponge *Homaxinella* sp. J Nat Prod 68:331–336
18. Stahelin H (1973) Activity of a new glycosidic ligan derivative (VP 16–213) related to podophyllotoxin in experimental tumors. Eur J Cancer 9:215–221
19. Nissen NI, Hansen HH, Pederson H, Stroyer I, Dombernowsky P, Hessllund M (1975) Clinical trial of the oral form of a new podophyllotoxin derivative, VP 16–213 (NSC-141540), in patients with advanced neoplastic disease. Cancer Chemother Rep 59:1027–1029
20. Issell BF, Crooke ST (1979) Etoposide (VP 16–213). Cancer Treat Rev 6:107–124
21. Yue J, Chen Z, Lin Z, Sun H (2001) Sterols from the fungus *Lactarium volemus*. Phytochemistry 56:801–806
22. Chen R, Wang Y, Yu D (1991) Chemical constituents of the spores from *Ganoderma lucidum*. Acta Botanica Sinica 33:65–68

α-Synuclein Aggregation and Transmission Are Enhanced by Leucine-Rich Repeat Kinase 2 in Human Neuroblastoma SH-SY5Y Cells

Kazunari KONDO,* Saemi OBITSU, and Reiko TESHIMA

National Institute of Health Sciences, Division of Novel Foods and Immunochemistry; 1–18–1 Kamiyoga, Setagaya-ku, Tokyo 158–8501, Japan. Received February 16, 2011; accepted March 30, 2011; published online April 14, 2011

Formation of α-synuclein aggregates is a key step in Parkinson's disease pathogenesis although the etiology remains elusive. α-Synuclein is accumulated in degenerating neurons, leading to the production of filamentous inclusions such as Lewy bodies. However, the *in vitro* overexpression of α-synuclein alone failed to induce inclusion bodies consisting of phosphorylated α-synuclein. The seeded aggregates-initiated polymerization of α-synuclein and tau has been reported elsewhere. What molecule is an initiator of filamentous inclusions remains to be defined. Here, we report that leucine-rich repeat kinase 2 (LRRK2)-cotransfection together with α-synuclein enhance the aggregate formation, phosphorylation, release to extracellular media of α-synuclein, and the cell-to-cell transmission into neighboring cells in human neuroblastoma SH-SY5Y cells. In cells transfected with α-synuclein alone, the proteins were distributed in the cytosol and did not form inclusions. On the other hand, the inclusions and phosphorylation of α-synuclein were formed in cells cotransfected with α-synuclein and LRRK2 G2019S mutant together. LRRK2 G2019S-cotransfected PC12 cells also induced the aggregates. Furthermore, the cell-to-cell transmission of α-synuclein and the cell toxicity were also enhanced by either LRRK2 wild type or G2019S mutant, whereas the cell viability was not decreased in cells transfected with α-synuclein alone. These results suggest that overexpression of LRRK2, especially G2019S mutant, whose functions remain unclear, initiate the aggregate formation, release and transmission of α-synuclein, resulting in the propagation of α-synuclein to neighboring cells and reduction of cell viability.

Key word α-synuclein; leucine-rich repeat kinase-2; aggregation; cell-to-cell transmission

Parkinson disease (PD) is the second most common neurodegenerative disease. The muscle rigidity, tremor, and bradykinesia that are characteristic of PD patients, are caused by dopaminergic neuron death in the substantia nigra. One of the well-known pathological hallmarks inside the cells is the presence of inclusion bodies called Lewy bodies (LB) that include aggregates of α-synuclein. Since α-synuclein and leucine-rich repeat kinase 2 (LRRK2) cause familial forms of PD that resembles sporadic PD pathologically, these genetic mutations provide important molecular tools to investigate PD pathogenesis.[1] Although the etiology of PD remains unclear, the production of aggregated α-synuclein is a key step in PD pathogenesis.[2]

α-Synuclein plays an important role in PD pathology and neuronal cell death.[3—5] Point mutations (A30P, E46K, and A53T) and multiplication of the gene α-synuclein are linked to the early-onset of PD pathology. The increased severity of PD and earlier age of onset have been reported to correlate with increased α-synuclein dosage.[6] The physiological function of α-synuclein found in pre-synapus remains undefined. Several studies have indicated that α-synuclein regulates intracellular transport of synaptic vesicles underlying neurotransmitter release.[7—14] α-Synuclein may also be involved in mitochondrial complex I function,[15,16] and has been reported to impair macroautophagy.[17]

Until recently, α-synuclein was considered to exert pathogenic effects inside the cells. However, α-synuclein can be detected in human cerebrospinal fluid (CSF) and plasma.[18] The accumulation of aggregated α-synuclein spreads from lower brainstem into the limbic system and neocortex, suggesting a mechanism underlying pathological propagation of PD such as Prion diseases.[19] Some groups have reported that aggregated α-synuclein can be released into extracellular media by exocytosis through exosomes and propagated by direct neuron-to-neuron transmission.[20—22]

LRRK2 is a large 2527 amino acid protein consisting of several functional domains including a Ras-like small GTPase domain (ROC), a carboxy-terminal of Roc (COR) domain, and a kinase domain. The various mutations in LRRK2 are involved in PD, such as R1441C, R1441G in the Roc domain, Y1699C in the COR domain, and G2019S, I2020T in the kinase domain. Among them, G2019S mutation clearly increases kinase activity, which is required for PD pathology.[23,24] G2019S mutation has been shown to increase kinase activity by 2 to 3 fold. However, normal function and kinase substrates of LRRK2 remain unclear. Although mutant LRRK2 was toxic when overexpressed in cultured cells[25,26] and *Drosophila*,[27,28] loss of neurons was not observed in transgenic mice overexpressing R1441G and R1441C mutants.[29,30] Loss of LRRK2 did not cause neurodegeneration and neuropathological changes. LRRK2 mutations cause clinically typical PD features, ranging from nigral degeneration without LB to nigral degeneration with widespread LB or neurofibrillary tangles.[31]

The neuronal cell death through neuron-to-neuron transmission of α-synuclein has been reported using mouse cortical neuron stem cells.[22] Coexpression of LRRK2 with A53T mutant of α-synuclein causes synergistic toxicity to neurons that accelerate the progression of α-synuclein-mediated pathology.[29] However, the underlying mechanism has not been yet defined. Thus, we have investigated the aggregate formation and cell-to-cell transmission of α-synuclein and the toxicity in the presence of LRRK2 wild type (WT) and G2019S mutant.

MATERIAL AND METHODS

Materials The antibody (Ab) for α-synuclein (mouse

* To whom correspondence should be addressed. e-mail: kondo@nihs.go.jp

immunoglobulin G_1 (IgG_1)) was purchased from BD Biosciences. Anti-phospho α-synuclein (clone #64) was obtained from Wako Pure Chemical (Japan). Anti-β-actin was purchased from Santa Cruz Biotechnology. Extracellular signal-regulated kinase 1/2 (ERK1/2) was purchased from Cell Signaling. Anti-LRRK2 (C-terminal region) was obtained from Sigma-Aldrich. MitoTracker Red CMX-H_2Ros to stain mitochondria in live cells and Lipofectamin 2000 were purchased from Invitrogen. cDNA constructs for wild type α-synuclein, α-synuclein A53T mutant, and enhanced green fluorescent protein (EGFP)-α-synuclein were kindly gifted by Dr. Sang Myun Park (Ajou University School of Medicine, Korea). c-Myc-tagged (2×myc) LRRK2 WT, G2019S, and kinase dead (KD) were kindly gifted by Dr. Mark Cookson (NIH, Bethesda). All sequences of the plasmids were confirmed. Transfection was performed by the method of lipofection (Lipofectamin 2000, Invitrogen) or electroporation (Amaxa Nucleofactor II, Lonza).

Cell Culture Human neuroblastoma SH-SY5Y cells (American Type Culture Collection [ATCC], CRL-2266) were grown in Dulbecco's modified Eagle's medium (DMEM)/F-12 supplemented with 10% fetal calf serum (FCS) penicillin, and streptomycin (Invitrogen). The SH-SY5Y was induced to differentiate by the treatment with 10 μM all-*trans* retinoic acid (RA, Sigma-Aldrich) and maintained at 37 °C and 5% CO_2. PC12 (JCRB0266) cells were grown in DMEM supplemented with 10% horse serum and 5% FCS, penicillin, and streptomycin (Invitrogen). The cell viability was measured by a WST-8 assay (Nacalai Tesque, Japan). Briefly, SH-SY5Y cells were transfected and differentiated by RA for 24 h to 8 d for cell viability assay. At the indicated times, the cell count reagent (2-(2-methoxy-4-nitrophenyl)-3-(4-nitrophenyl)-5-(2,4-disulfophenyl)-2*H*-tetrazolium) for the WST-8 assay was added to the cells, and the cells were incubated for 2—4 h. Cell viability was measured by 450 nm and 650 nm (as a reference) absorbance. Cell viability data were obtained from three independent experiments performed in triplicate.

For α-synuclein transmission experiments, cells were transfected with EGFP-α-synuclein with or without LRRK2 by electroporation (1×10^6 cells/electroporation), and cultured for 24 or 48 h in 24-well culture plates. At 24 h, the conditioned media were collected, centrifuged at 3000 ***g*** for 10 min to remove dead cells and cell debris. The supernatants were transferred to separately prepared SH-SY5Y cells in the differentiation condition. The cells were cultured for another 24 h to 8 d, and the cell viabilities were measured by WST-8 assay.

Western Blot Analysis SH-SY5Y cells were cultured at 9×10^5 cells/dish in 10-cm dishes in the differentiation condition following the transfection of α-synuclein with or without LRRK2. At 24 or 48 h-posttransfection, the cells were rinsed with Tris-buffered saline (TBS), and cell lysates were prepared using Triton-based lysis buffer containing protease and phosphatase inhibitors. The cell lysates were resolved by sodium dodecyl sulfate/polyacrylamide gel electrophoresis (SDS/PAGE) on 5—20% gradient gels, and transferred onto polyvinylidene fluoride (PVDF) membranes (ATTO, Japan). The membranes were incubated with primary Abs at 4 °C overnight, and then with alkaline phosphatase (AP)-labeled secondary Abs for 1 h at room temperature. The blots were detected by an AP-conjugated substrate kit (BioRad), and the images were scanned and analyzed using Photoshop CS5. For the detection of α-synuclein in the conditioned media, chemiluminescent ECL system was used to detect the blots (ECL plus, GE Healthcare). The blots were analyzed using ImageQuant LAS-4000 (Fujifilm, Japan). Western blot analyses were performed on data from three independent experiments.

Immunofluorescent Staining SH-SY5Y cells on glass chamber slides were washed twice with DPBS before the cells were fixed with 4% paraformaldehyde (Wako, Japan) for 30 min and permeabilized with cold 0.2% Triton X-100 for 10 min. After blocking with 2% bovine serum albumin (BSA) for 1 h, the cells were incubated with primary Abs against α-synuclein, phosphor-α-synuclein, LRRK2, ERK, or β-actin at 4 °C overnight. MitotrackerRed CMX-H_2Ros was used to stain mitochondria of the live cells. The cells were washed and incubated with Alexa 488- or Alexa 555-labeled secondary Abs (Invitrogen) and Hoechst 33342 (Invitrogen) at room temperature for 1 h. After washing, the cells were mounted with Prolong gold mounting media (Invitrogen). Fluorescent microscopy was performed using an IX71 microscope (Olympus, Japan) and CarlZeiss LSM-Pascal (Germany). Immunofluorescent staining data were obtained from more than three independent experiments.

Transfection of α-Synuclein and LRRK2 SH-SY5Y cells (1×10^6 cells/cuvette) were transfected with α-synuclein, α-synuclein A53T, or EGFP-α-synuclein (1.5 μg cDNA each), and LRRK2 (1.5 μg cDNA) using Amaxa (program #A023, Lonza, Switzerland). The transfected cells were seeded to 10-cm culture dishes for Western blotting or 24-well culture plates for immunofluorescence and cell viability assay, and cultured for 24 to 8 d in the differentiation condition. PC12 cells were seeded at 0.25×10^5 cells/ml into a polylysine-coated 24 well plate (BD Biosciences). The cells were transfected using cDNA (0.5 μg each) and lipofectamine 2000 (Invitrogen) in OPTI-MEM (Invitrogen), and cultured for 24 h. Then, the cells were differentiated with nerve growth factor (NGF) (50 ng/ml), and cultured for another 4 d.

Statistical Analysis All data are expressed as the mean±standard deviation (S.D.). The statistical significance was evaluated by one-way analysis of variance (ANOVA) followed by the Dunnett's test to compare the data from multiple groups against a common control group. Student's *t*-test was used to compare the data from two groups (SigmaPlot). Statistical significance was determined at $p<0.05$ (indicated with an asterisk in the figures).

RESULTS

Formation of α-Synuclein Aggregates and Cell-to-Cell Transmission SH-SY5Y cells were transfected with wild type (WT) α-synuclein fused with EGFP by lipofection or electroporation in the proliferating or differentiation conditions, respectively. In proliferating cells, EGFP-α-synuclein was distributed in the cytoplasm 24 h after lipofection. By 48 h, the α-synuclein-containing vesicles were increased around the cells. A larger amount of vesicles was observed on the surface and outside of the cells 72 h after transfection (Fig. 1A). In the differentiation condition, α-synuclein-containing vesicles were not produced in the cells transfected

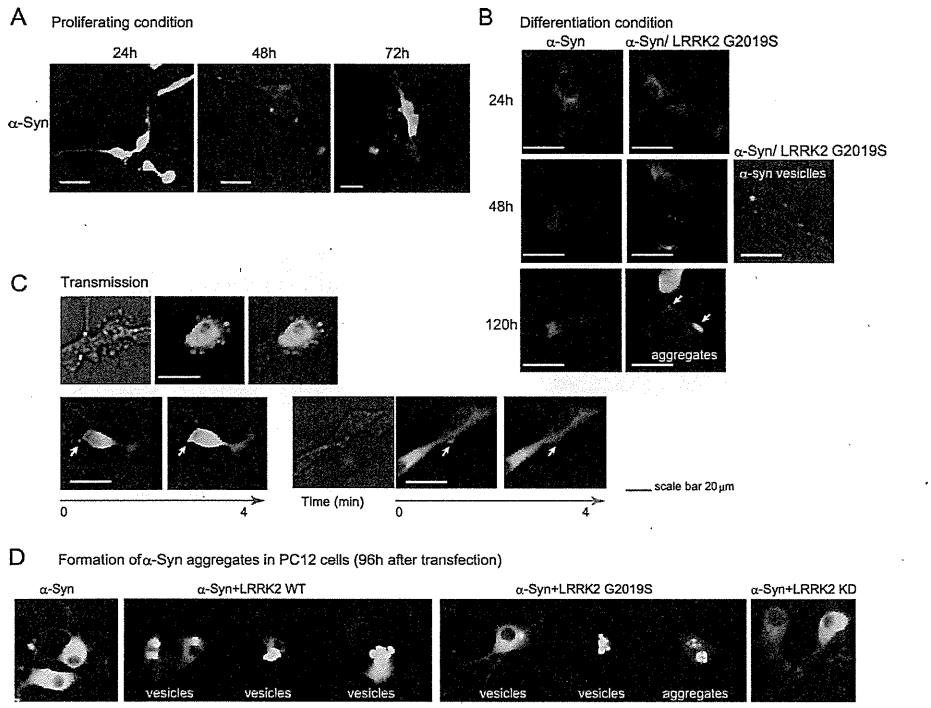

Fig. 1. Aggregate Formation and Vesicle Movement of α-Synuclein

SH-SY5Y cells were transfected with α-synuclein alone or with LRRK2 G2019S mutant in the proliferating and differentaion conditions. (A) α-Synuclein was localized in the cytoplasm in α-synuclein-transfected cells. (B) α-Synuclein was distributed in the cytoplasm, and many vesicles were formed and on the surface of neighboring cells within 48 h after transfection in RA-differentiated cells. In the presence of LRRK2 G2019S, α-synuclein aggregates were produced inside the cells after 5 d-culture (white arrow). (C) α-Synuclein-containing vesicles were moved into neighboring cells by cell contact (bottom left) or direct transmission through the conditioned media (bottom right). (D) Similar experiments were performed using the differentiated PC12 cells. LRRK2 WT-cotransfected cells have large vesicles containing α-synuclein, which appear to be effluxed from the cells. Cells cotransfected with LRRK2 G2019S did have the aggregates of α-synuclein.

with α-synuclein alone, whereas the vesicles and aggregates were formed in the cells cotransfected with α-synuclein and LRRK2 G2019S (Fig. 1B). The aggregated α-synuclein was also observed in RA-differentiated SH-SY5Y cells. The large aggregates were formed inside the cell 120 h after cotransfection of α-synuclein and LRRK2 G2019S mutant (Fig. 1B, white arrow). Since the aggregated proteins and vesicles of α-synuclein were found inside and on the surface of the cells, transmission of α-synuclein from one cell to neighboring cells was next investigated in the differentiated SH-SY5Y cells. A single EGFP-labeled α-synuclein was moving toward the neighboring cell or through the conditioned media, and appeared to be internalized on the cell surface (Fig. 1C). Many vesicles were exocytosed through plasma membrane (Fig. 1C, top). For further studies, we used rat adrenal pheochromocytoma PC12cells to evaluate the effect of LRRK2 on α-synuclein aggregation. In cells cotransfected with α-synuclein and LRRK2 WT, large vesicles releasing from the cells at the very moment were observed at 96 h posttransfection. Although similar vesicles containing α-synuclein were seen in PC12 cells cotransfected with LRRK2 G2019S mutant, distinct aggregates were also observed in the nucleus. In contrast, LRRK2 KD-transfected cells did not have any large vesicles and aggregates.

Taken together, α-synuclein-containing vesicle formation was enhanced by LRRK2 WT or G2019S mutant. α-synuclein aggregates were induced only by LRRK2 G2019S mutant.

α-Synuclein Transmission Is Enhanced in the Presence of LRRK2 G2019S Mutant Next, we investigated the effect of LRRK2 G2019S mutant on α-synuclein transmission. α-Synuclein alone or with LRRK2 WT or G2019S mutant was transfected into SH-SY5Y cells by electroporation, and cultured for 48 h in the differentiation condition. The supernatant of the conditioned media collected from the transfected cells was added to separately prepared and RA-differentiated SH-SY5Y cells without any concentration. Then, the cells were incubated for another 24—48 h to observe the expression of α-synuclein in the untransfected cells (Fig. 2A). The ratio of α-synuclein-expressed cells to total untransfected cells in the area that includes 300 cells was measured. Approximately 5% of cells were GFP-positive (4.7±1.2%) when the conditioned media from α-synuclein-transfected cells was transferred into the separately prepared cells, whereas 11% of cells were GFP-positive (10.7±2.1%) when the media from cells cotransfected with α-synuclein and LRRK2 G2019S was used as shown in Fig. 2A. The number of GFP-positive cells in the presence of LRRK2 G2019S mutant was greater than that in the absence of LRRK2 mutant.

To confirm that α-synuclein protein was internalized by the separately prepared cells, separately prepared and RA-differentiated SH-SY5Y cells were labeled with MitotrackerRed CMX-H_2Ros in advance, which is sensitive to mitochondrial membrane potential. α-Synuclein was indeed incorporated into the untransfected cells (Fig. 2B). The expression of α-synuclein was increased in a time-dependent manner, and there was no difference in α-synuclein expression between α-synuclein wild type and A53T mutant at 24 and 48 h (Fig. 2C). α-Synuclein expression was increased in

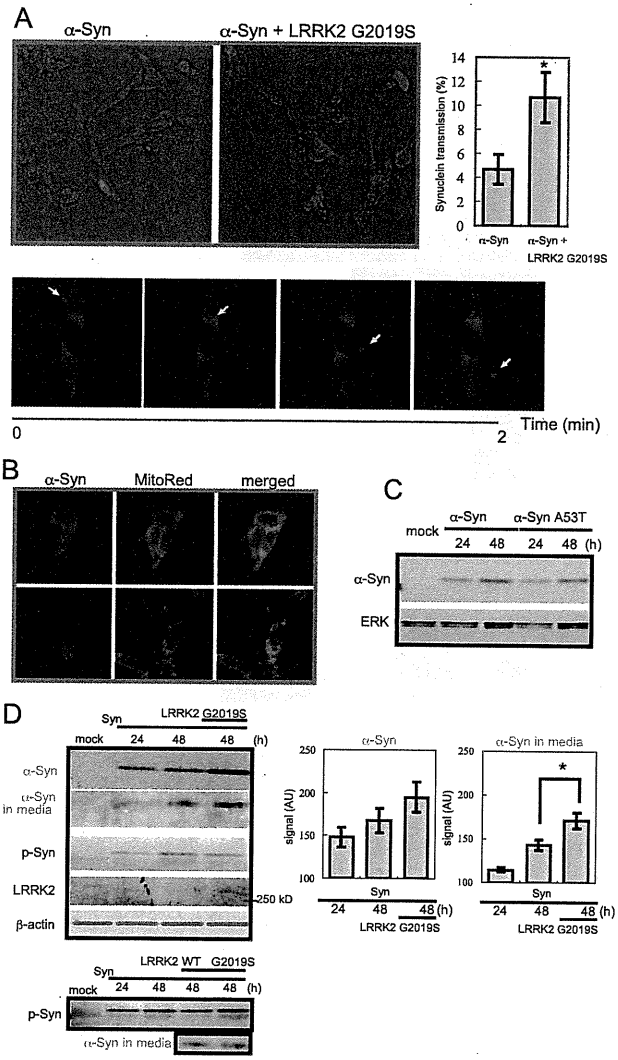

Fig. 2. α-Synuclein Transmission Is Enhanced by LRRK2

The conditioned media from α-synuclein-transfected cells in the presence or absence of LRRK2 were added to the separately prepared cells, and cultured for another 24 h to clarify whether α-synuclein proteins are incorporated into neighboring cells through the conditioned media. (A) The untransfected SHSY5Y cells were cultured in the conditioned media collected from α-synuclein-transfected cells. Transmission of α-synuclein from α-synuclein-transfected cells to separately prepared and untransfected cells was enhanced by LRRK2 G2019S mutant. The ratio of transmission in the presence of LRRK2 was greater than that in the absence of LRRK2. Three hundred cells from different wells of a 24-well culture plate were counted in each experiment. The data were obtained from three independent experiments (n=3, $*p<0.05$). One α-synuclein-containing vesicle is moving and crossing over the cells in the conditiond media. (B) α-Synuclein proteins were incorporated into the untransfected and MitotrackerRed-labeled cells, showing the transmission through the media. Two different fields were shown here. (C) α-Synuclein was expressed in the α-synuclein-transfected cells in a time-dependent manner. There was no difference between α-synuclein wild type and A53T mutant in the expression. (D) α-Synuclein expression inside the cells and in the conditioned media in the presence of LRRK2 WT and G2019S. A larger amount of α-synuclein was detected in the conditioned media from LRRK2 G2019S-expressing cells. There was no difference between LRRK2 WT and G2019S-expressing cells. The amounts of phosphorylated α-synuclein were not significant in transfected cells. The data were obtained from two to three independent experiments (n=2 or 3). Representatives were shown in Western blots.

cells cotransfected with LRRK2, but not significant (Fig. 2D). The expression of α-synuclein was also confirmed in the conditioned media from SH-SY5Y cells transfected with α-synuclein alone or with LRRK2 WT or G2019S. α-Synuclein was detected in the media within 24 h and increased with the time (Fig. 2D). LRRK2 G2019S mutant did significantly enhance the α-synuclein release into the conditioned media. However, the amount of α-synuclein in the conditioned media was not significantly different between LRRK2 WT and G2019S mutant. The phosphorylation state was not different between the two groups either (Fig. 2D, bottom).

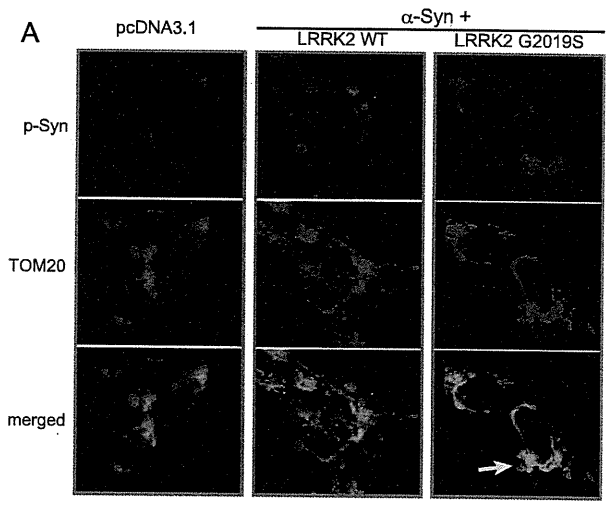

Fig. 3. α-Synuclein Localization and Its Phosphorylation

α-Synuclein (green) aggregates were phosphorylated and localized in mitochondria (red) in LRRK2 G2019S-trasnfected cells (white arrow). Large vesicles of α-synuclein were phosphorylated but not localized in LRRK2 WT-transfected cells. Cells transfected with pcDNA 3.1 did not have any aggregates and vesicles.

Aggregated α-Synuclein Is Phosphorylated and Localized in Mitochondria We next examined the phosphorylation state and its localization of aggregated α-synuclein by staining with a mitochondria outer-membrane marker TOM20. As shown in Fig. 3, most of the aggregated α-synuclein were phosphorylated and colocalized with mitochondria in the differentiated SH-SY5Y cells coexpressing α-synuclein and LRRK2 G2019S mutant (white arrow). The phosphorylated α-synuclein-containing vesicles were seen in LRRK2 WT-transfected cells, but not colocalized with mitochondria. The pcDNA3.1-transfected cells did not have any vesicles and aggregates.

Cell Viabilities in α-Synuclein and LRRK2-Cotransfected Cells The cell viabilities of SH-SY5Y cells cotransfected with α-synuclein and LRRK2 wild type or LRRK2 G2019S mutant were investigated. When the cells were transfected with α-synuclein alone, the viability was not significantly different from that of the cells treated with pcDNA3.1 as a control. Like wild type, α-synuclein A53T mutant alone did not show the decrease in the cell viability during 8 d-culture. These results suggest that α-synuclein alone do not lead to the cell death for several days (Fig. 4). However, when the cells were cotransfected with α-synuclein and LRRK2 WT or G2019S mutant, the viabilities decreased by 12%, suggesting that LRRK2 enhance the cell toxicity by α-synuclein (Fig. 4). In addition, the cell toxicity was not observed in LRRK2 G2019S-mutant transfected SH-SY5Y. These results indicate that LRRK2 synergistically reduce the cell viability of α-synuclein-tranfected cells.

DISCUSSION

Until several years ago, α-synuclein was considered an

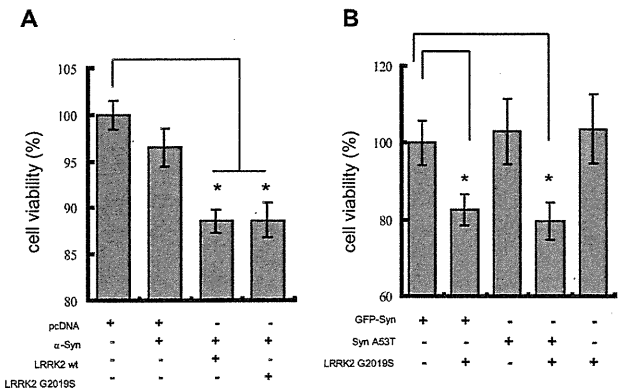

Fig. 4. Cell Viability of the Cells Transfected with α-Synuclein Alone or with LRRK2

(A) Cell viability was significantly decreased in the presence of LRRK2 WT or G2019S. There is no difference between WT and G2019S of LRRK2. (B) α-Synuclein WT and A53T mutant alone had no effect on the cell viability, whereas the viability was decreased in the presence of LRRK2 G2019S mutant. The data were three (A) and four (B) independent experiments in triplicates ($*p<0.05$).

intracellular protein and to function cell-autonomously. Recently, α-synuclein was reported to be present in human cerebrospinal fluid (CSF) and human plasma at a concentration of nanomolar in PD and normal subjects.[18,32] Two studies showed host-to-graft propagation of α-synuclein-positive Lewy-like pathology in long-term mesencephalic transplants in PD.[33,34] Most recently, cell-to-cell transmission of α-synuclein and the resulting cell death in neuronal cells has been demonstrated by Desplats *et al.*[22] In addition, Lin *et al.* has reported that LRRK2 enhances α-synuclein-mediated cytotoxicity.[29] Therefore, these results above now raise the question how LRRK2 give rise to the synergistic effect in cytotoxicity. Here, we have investigated the effect of α-synuclein aggregation and transmission in the presence of LRRK2 WT, G2019S, and KD.

α-Synuclein was distributed in the cytosol and many secreted vesicles including α-synuclein were observed outside and on the surface of SH-SY5Y cells by 48 h after transfection. The large aggregates were produced by 5 d in the cells cotransfected with α-synuclein and LRRK2 G2019 mutant, whereas such a large aggregate was not produced in the cells transfected with α-synuclein alone or with LRRK2 WT. The accumulation and propagation of amyloid β proteins are thought to occur through nucleation-dependent polymerization. Recently, the seed-dependent aggregate formation of α-synuclein has been reported using lipofection of seeded aggregation.[35] This may be an excellent model. However, the question where the first aggregates come from remains to be answered. We present here that LRRK2 G2019S initiates and enhances the formation of α-synuclein aggregates. Furthermore, vesicles including α-synuclein were transmitted to neighboring cells through the conditioned media especially in the presence of LRRK2. Intercellular transmission of exogenous protein aggregates has been well documented in Prion disorder. Similar mechanisms of pathological propagation have been suggested in other neurodegenerative diseases such as Alzheimer's and Polyglutamine diseases.[36,37] Extracellular tau aggregates also has been shown to induce the aggregation of intracellular protein.[38] Therefore, cell-to-cell transmission of aggregated proteins may be the common feature underlying progressive neurodegenerative diseases. Lin *et al.* has recently reported an important functional interplay between α-synuclein and LRRK2 in the development of neurodegeneration. LRRK2 accelerates the progression of neuropathological abnormality.[29] Our results were well consistent with this report. In the present study, larger amounts of α-synuclein were present in the conditioned media upon cotransfection of α-synuclein and LRRK2, compared to the amounts upon transfection of α-synuclein alone. These results suggest that LRRK2 enhance the α-synuclein release to extracellular media and the aggregate formation of α-synuclein. Tong *et al.* have recently reported that loss of LRRK2 causes the accumulation of α-synuclein only in kidney, not in neuronal cells.[30] The effect of LRRK2 might be dependent on cell types. We need to investigate how only LRRK2 G2019S initiates the aggregates for further study.

Here we show an interesting finding that LRRK2 G2019S enhances aggregate formation and transmission of α-synuclein and the cell toxicity.

Acknowledgements This work was supported by Grant from the Japan Health Sciences Foundation (KHB1201 to R. T.) and Grant-in-Aid for Scientific Research from the Ministry of Education, Culture, Sports, Science and Technology of Japan (20590132 to K. K.).

REFERENCES

1) Hardy J., *Mov. Disord.*, **2006**, 1790—1791 (2006).
2) Trojanowski J. Q., Goedert M., Iwatsubo T., Lee V. M.-Y., *Cell Death Differ.*, **5**, 832—837 (1998).
3) Dawson T. M., Dawson V. L., *Science*, **302**, 819—822 (2003).
4) Shults C. W., *Proc. Natl. Acad. Sci. U.S.A.*, **103**, 1661—1668 (2006).
5) Lees A. J., Hardy J., Revesz T., *Lancet*, **373**, 2055—2066 (2009).
6) Ross O. A., Braithwaite A. T., Skipper L. M., Kachergus J., Hulihan M. M., Middleton F. A., Nishioka K., Fuchs J., Gasser T., Maraganore D. M., Adler C. H., Larvor L., Chartier-Harlin M. C., Nilsson C., Langston J. W., Gwinn K., Hattori N., Farrer M. J., *Ann. Neurol.*, **63**, 743—750 (2008).
7) Abeliovich A., Schmitz Y., Farinas I., Choi-Lundberg D., Ho W. H., Castillo P. E., Shinsky N., Verdugo J. M., Armanini M., Ryan A., Hynes M., Phillips H., Sulzer D., Rosenthal A., *Neuron*, **25**, 239—252 (2000).
8) Ben Gedalya T., Loeb V., Israeli E., Altschuler Y., Selkoe D. J., Sharon R., *Traffic*, **10**, 218—234 (2009).
9) Cabin D. E., Shimazu K., Murphy D., Cole N. B., Gottschalk W., Mc Ilwain K. L., Orrison B., Chen A., Ellis C. E., Paylor R., Lu B., Nussbaum R. L., *J. Neurosci.*, **22**, 8797—8807 (2002).
10) Cooper A. A., Gitler A. D., Cashikar A., Haynes C. M., Hill K. J., Bhullar B., Liu K., Xu K., Strathearn K. E., Liu F., Cao S., Caldwell K. A., Caldwell G. A., Marsischky G., Kolodner R. D., Labaer J., Rochet J. C., Bonini N. M., Lindquist S., *Science*, **313**, 324—328 (2006).
11) Murphy D. D., Rueter S. M., Trojanowski J. Q., Lee V. M., *J. Neurosci.*, **20**, 3214—3220 (2000).
12) Nemani V. M., Lu W., Berge V., Nakamura K., Onoa B., Lee M. K., Chaudhry F. A., Nicoll R. A., Edwards R. H., *Neuron*, **65**, 66—79 (2010).
13) Sousa V. L., Bellani S., Giannandrea M., Yousuf M., Valtorta F., Meldolesi J., Chieregatti E., *Mol. Biol. Cell*, **20**, 3725—3739 (2009).
14) Yavich L., Tanila H., Vepsäläinen S., Jäkälä P., *J. Neurosci.*, **24**, 11165—11170 (2004).
15) Devi L., Raghavendran V., Prabhu B. M., Avadhani N. G., Anandatheerthavarada H. K., *J. Biol. Chem.*, **283**, 9089—9100 (2008).
16) Loeb V., Yakunin E., Saada A., Sharon R., *J. Biol. Chem.*, **285**, 7334—7343 (2010).
17) Winslow A. R., Chen C. W., Corrochano S., Acevedo-Arozena A., Gordon D. E., Peden A. A., Lichtenberg M., Menzies F. M., Ravikumar B., Imarisio S., Brown S., O'Kane C. J., Rubinsztein D. C., *J. Cell*

Biol., **190**, 1023—1037 (2010).
18) El-Agnaf O. M., Salem S. A., Paleologou K. E., Cooper L. J., Fullwood N. J., Gibson M. J., Curran M. D., Court J. A., Mann D. M., Ikeda S., Cookson M. R., Hardy J., Allsop D., *FASEB J.*, **17**, 1945—1947 (2003).
19) Frost B., Diamond M. I., *Nat. Rev. Neurosci.*, **11**, 155—159 (2010).
20) Emmanouilidou E., Melachroinou K., Roumeliotis T., Garbis S. D., Ntzouni M., Margaritis L. H., Stefanis L., Vekrellis K., *J. Neurosci.*, **30**, 6838—6851 (2010).
21) Lee H. J., Patel S., Lee S. J., *J. Neurosci.*, **25**, 6016—6024 (2005).
22) Desplats P., Lee H. J., Bae E. J., Patrick C., Rockenstein E., Crews L., Spencer B., Masliah E., Lee S. J., *Proc. Natl. Acad. Sci. U.S.A.*, **106**, 13010—13015 (2009).
23) Cookson M. R., Dauer W., Dawson T., Fon E. A., Guo M., Shen J., *J. Neurosci.*, **27**, 11865—11868 (2007).
24) Cookson M. R., *Nat. Rev. Neurosci.*, **11**, 791—797 (2010).
25) Greggio E., Jain S., Kingsbury A., Bandopadhyay R., Lewis P., Kaganovich A., van der Brug M. P., Beilina A., Blackinton J., Thomas K. J., Ahmad R., Miller D. W., Kesavapany S., Singleton A., Lees A., Harvey R. J., Harvey K., Cookson M. R., *Neurobiol. Dis.*, **23**, 329—341 (2006).
26) Smith W. W., Pei Z., Jiang H., Dawson V. L., Dawson T. M., Ross C. A., *Nat. Neurosci.*, **9**, 1231—1233 (2006).
27) Imai Y., Gehrke S., Wang H. Q., Takahashi R., Hasegawa K., Oota E., Lu B., *EMBO J.*, **27**, 2432—2443 (2008).
28) Liu Z., Wang X., Yu Y., Li X., Wang T., Jiang H., Ren Q., Jiao Y., Sawa A., Moran T., Ross C. A., Montell C., Smith W. W., *Proc. Natl. Acad. Sci. U.S.A.*, **105**, 2693—2698 (2008).
29) Lin X., Parisiadou L., Gu X. L., Wang L., Shim H., Sun L., Xie C., Long C. X., Yang W. J., Ding J., Chen Z. Z., Gallant P. E., Tao-Cheng J. H., Rudow G., Troncoso J. C., Liu Z., Li Z., Cai H., *Neuron*, **64**, 807—827 (2009).
30) Tong Y., Yamaguchi H., Giaime E., Boyle S., Kopan R., Kelleher R. J. 3rd, Shen J., *Proc. Natl. Acad. Sci. U.S.A.*, **107**, 9879—9884 (2010).
31) Tong Y., Shen J., *Neuron*, **64**, 771—773 (2009).
32) Borghi R., Marchese R., Negro A., Marinelli L., Forloni G., Zaccheo D., Abbruzzese G., Tabaton M., *Neurosci. Lett.*, **287**, 65—67 (2000).
33) Li J. Y., Englund E., Holton J. L., Soulet D., Hagell P., Lees A. J., Lashley T., Quinn N. P., Rehncrona S., Björklund A., Widner H., Revesz T., Lindvall O., Brundin P., *Nat. Med.*, **14**, 501—503 (2008).
34) Kordower J. H., Chu Y., Hauser R. A., Freeman T. B., Olanow C. W., *Nat. Med.*, **14**, 504—506 (2008).
35) Nonaka T., Watanabe S. T., Iwatsubo T., Hasegawa M., *J. Biol. Chem.*, **285**, 34885—34898 (2010).
36) Frost B., Diamond M. I., *Nat. Rev. Neurosci.*, **11**, 155—159 (2010).
37) Caughey B., *Nat. Med.*, **6**, 751—754 (2000).
38) Frost B., Jacks R. L., Diamond M. I., *J. Biol. Chem.*, **284**, 12845—12852 (2009).

THE JOURNAL OF BIOLOGICAL CHEMISTRY VOL. 285, NO. 17, pp. 13079–13091, April 23, 2010

Poly(ADP-ribose) Polymerase (PARP)-1-independent Apoptosis-inducing Factor (AIF) Release and Cell Death Are Induced by Eleostearic Acid and Blocked by α-Tocopherol and MEK Inhibition*[S]

Received for publication, July 14, 2009, and in revised form, February 2, 2010 Published, JBC Papers in Press, February 22, 2010, DOI 10.1074/jbc.M109.044206

Kazunari Kondo[‡1], Saemi Obitsu[‡], Sayaka Ohta[‡], Katsuyoshi Matsunami[§], Hideaki Otsuka[§], and Reiko Teshima[‡]

From the [‡]Division of Novel Food and Immunochemistry, National Institute of Health Sciences, 1-18-1 Kamiyoga, Setagaya, Tokyo 158-8501 and the [§]Department of Pharmacognosy, Graduate School of Biomedical Sciences, Hiroshima University, 1-2-3 Kasumi, Minami-ku, Hiroshima 734-8553, Japan

Poly(ADP-ribose)polymerase-1 (PARP-1) is thought to be required for apoptosis-inducing factor (AIF) release from mitochondria in caspase-independent apoptosis. The mechanism by which AIF is released through PARP-1 remains unclear. Here, we provide evidence that PARP-1-independent AIF release and cell death are induced by a trienoic fatty acid, α-eleostearic acid (α-ESA). α-ESA induced the caspase-independent and AIF-initiated apoptotic death of neuronal cell lines, independently of PARP-1 activation. The cell death was inhibited by the MEK inhibitor U0126 and by knockdown of MEK using small interfering RNA. However, inhibitors for JNK, p38 inhibitors, calpain, phospholipase A_2, and phosphatidylinositol 3-kinase, did not block cell death. AIF was translocated to the nucleus after the induction of apoptosis by α-ESA in differentiated PC12 cells without activating caspase-3 and PARP-1. The α-ESA-mediated cell death was not inhibited by PARP inhibitor 3,4-dihydro-5-[4-(1-piperidinyl)butoxyl]-1(2*H*)-isoquinoline and by knockdown of PARP-1 using small interfering RNA. Unlike *N*-methyl-*N*′-nitro-*N*-nitrosoguanidine treatment, histone-phosphorylated histone 2AX was not phosphorylated by α-ESA, which suggests no DNA damage. Overexpression of Bcl-2 did not inhibit the cell death. α-ESA caused a small quantity of superoxide production in the mitochondria, resulting in the reduction of mitochondrial membrane potential, both of which were blocked by a trace amount of α-tocopherol localized in the mitochondria. Our results demonstrate that α-ESA induces PARP-1-independent AIF release and cell death without activating Bax, cytochrome *c*, and caspase-3. MEK is also a key molecule, although the link between ERK, AIF release, and cell death remains unknown. Finding molecules that regulate AIF release may be an important therapeutic target for the treatment of neuronal injury.

Apoptosis is a mode of programmed cell death that is used by multicellular organisms to remove surplus and unwanted cells in the immune and nervous systems (1–5). Apoptosis is characterized by cell detachment, cell shrinkage, chromatin condensation, DNA degradation, and plasma membrane blebbing (5–7). The surplus cells are removed by caspases, which are key effector molecules of apoptotic cell death. Apoptosis is activated through two main pathways as follows: the extrinsic pathway, which originates from the activation of cell-surface death receptors, such as Fas and tumor necrosis factor-receptor 1, and results in the activation of caspase-8; and the intrinsic pathway, which originates from the mitochondrial release of cytochrome *c* and results in the activation of caspase-9 through the Cyt-c[2]/apoptotic protease-activating factor-1/procaspase-9 heptamer (5, 8, 9). Most apoptotic stimuli use a mitochondrion-dependent process such as membrane potential shutdown and outer membrane permeabilization controlled by Bax and Bak, which are pro-apoptotic members of the Bcl-2 family (6–9). This results in the release of the pro-apoptotic protein Cyt-c, which triggers caspase activation, or the apoptosis-inducing factor (AIF), which triggers caspase-independent pathways, from mitochondrial intermembrane space.

In the developing nervous system, apoptosis is necessary for the establishment of appropriate cell numbers and for the elimination of unwanted cells (10); however, in the adult nervous system, the inappropriate induction of apoptotic cell death contributes to neurodegenerative diseases (15, 16). Activation of the mitochondrial signaling cascade can activate both caspase-dependent and caspase-independent apoptosis (11, 12). AIF is a key molecule in caspase-independent neuronal cell death (13–16). AIF is released from the mitochondria into the cytosol and then translocated to the nucleus in response to neuronal

* This work was supported by grants from the Ministry of Health, Labor, and Welfare of Japan, the Japan Health Sciences Foundation, and Grant-in-aid for Scientific Research 20590132 (to K. K.).

[S] The on-line version of this article (available at http://www.jbc.org) contains supplemental Figs. S1 and S2 and Movie S1.

[1] To whom correspondence should be addressed. Tel.: 81-3-3700-1141; E-mail: kondo@nihs.go.jp.

[2] The abbreviations used are: Cyt-c, cytochrome *c*; α-ESA, α-eleostearic acid; MEK, mitogen-activated protein kinase kinase; JNK, c-Jun N-terminal kinase; ERK, extracellular signal-regulated kinase; γ-H2AX, phosphorylated histone 2AX; AIF, apoptosis-inducing factor; Bak, Bcl-2-antagonist/killer; Bax, Bcl-2-associated X protein; CPT, camptothecin; DPQ, 3,4-dihydro-5-[4-(1-piperidinyl)butoxyl]-1(2*H*)-isoquinoline; ERK, extracellular signal-regulated kinase; MEK, mitogen-activated protein kinase kinase; MNNG, *N*-methyl-*N*′-nitro-*N*-nitrosoguanidine; NGF, nerve growth factor; PARP-1, poly(ADP-ribose) polymerase-1; Z-, *N*-benzyloxycarbonyl; fmk, fluoromethyl ketone; ROS, reactive oxygen species; α-ESA, α-eleostearic acid; Ab, antibody; siRNA, small interfering RNA; TUNEL, terminal dUTP nick end-labeling; α-Toc, α-tocopherol; NMDA, *N*-methyl-D-aspartic acid; STS, staurosporine; JNK, c-Jun N-terminal kinase; PAR, polymer of ADP-ribose; CM-H2DCF-DA, 5(and 6)-chloromethyl-2′,7′-dichlorodihydrofluorescein diacetate; NBD, 7-nitro-2,1,3-benzoxadiazol-4-yl.

stimuli, including hypoxia, cerebral ischemia, and *N*-methyl-*N*′-nitrosoguanidine (MNNG) or *N*-methyl-D-aspartic acid (NMDA) insult (15, 17–20). Poly(ADP-ribose) polymerase-1 (PARP-1) activation is required for the translocation of AIF in fibroblasts (20). Moubarak *et al.* (21) has reported that the sequential activation of PARP-1, calpain, and Bax is essential in AIF-mediated programmed necrosis.

α-Eleostearic acid (α-ESA) is a conjugated trienoic fatty acid that occurs in the seeds of plants such as *Vernicia* spp. α-ESA has been reported to suppress tumor growth through caspase-3 and peroxisome proliferator-activated receptor-γ activation accompanied by DNA fragmentation (22–24). Recently, we have found that α-ESA induces caspase-independent apoptosis that is not associated with nucleosomal DNA fragmentation in neuronal cells. Notably, α-ESA-mediated apoptotic cell death is accompanied by AIF translocation to the nucleus and prolonged ERK phosphorylation that lasts for more than 16 h, but not by PARP-1 activation, in rat adrenal pheochromocytoma PC12 cells. The MEK inhibitor U0126 and a trace amount of α-tocopherol (α-Toc) completely inhibited the apoptotic cell death. The methyl ester of α-ESA (α-ESA-Me) did not induce apoptotic cell death, even though it has the same conjugated triene group as α-ESA. Here, we show that α-ESA causes PARP-1-independent AIF release and the cell death through the superoxide production in a small quantity in the mitochondria and the prolonged ERK1/2 phosphorylation without inducing other apoptotic molecules such as Bax, Bcl-2, Cyt-c, caspase-3, and PARP-1.

EXPERIMENTAL PROCEDURES

Cell Culture—PC12 (JCRB0266) cells were grown in Dulbecco's modified Eagle's medium supplemented with 10% horse serum and 5% fetal calf serum, penicillin, and streptomycin (Invitrogen). Human neuroblastoma (SH-SY5Y) cells (American Type Culture Collection (ATCC), CRL-2266) were grown in Dulbecco's modified Eagle's medium/F-12 supplemented with 10% fetal calf serum. Mouse neuroblastoma × rat glioma hybrid (NG108-15) cells (ATCC, HB-12317) were grown in Dulbecco's modified Eagle's medium supplemented with 10% fetal calf serum. The PC12 cells were induced to differentiate by treatment with 50 ng/ml NGF 7 S (Sigma) and were maintained at 37 °C and 5% CO_2. The SH-SY5Y and NG108-15 cells were induced to differentiate by treatment with 10 μM all-*trans*-retinoic acid (Sigma) and 250 μM dibutyryl cyclic AMP (Tocris), respectively. The PC12 and NG108-15 cells were allowed to differentiate on polylysine-coated plates or glass chambers. The cell viability was measured by a WST-8 assay (Nacalai Tesque, Japan). Briefly, PC12 cells were differentiated by NGF for 48 h, and then α-ESA was added to the cells. Sixteen hours later, the cell count reagent (2-(2-methoxy-4-nitrophenyl)-3-(4-nitrophenyl)-5-(2,4-disulfophenyl)-2*H* tetrazolium) for the WST-8 assay was added to the cells, and the cells were incubated for 1–2 h. For proliferating cells, α-ESA was added 16–18 h after seeding the cells. Cell viability was measured by 450 and 650 nm (as a reference) absorbance. When pretreatment with a specific inhibitor is needed, an inhibitor was added to the cells 30 min before α-ESA. Cell viability data were obtained between two and four independent experiments performed in triplicate.

Antibodies and Chemicals—The Abs for ERK, phospho-ERK, JNK/stress-activated protein kinase, phospho-JNK/stress-activated protein kinase, p38, phospho-p38, Akt, phospho-Akt, caspase-3, MEK1 (61B12), Bcl-2, and glyceraldehyde-3-phosphate dehydrogenase (14C10) were purchased from Cell Signaling. The Abs for AIF (E-1), Cyt-c (7H8), Bax (N-20), Bcl-2 (C-2), and PARP-1 (H-250) were purchased from Santa Cruz Biotechnology. Anti-PAR (10H) was obtained from Alexis Biochemicals. Anti-H2A was obtained from Millipore. Anti-γ-H2AX was obtained from Active Motif. Anti-manganese superoxide dismutase was obtained from Assay Designs. Anti-MEK2 was purchased from BD Biosciences. The pan-caspase inhibitor Z-VAD-fmk, PD98059, SB203580, U0126, palmitoyl trifluoromethyl ketone, and DPQ were obtained from Calbiochem. SP600125 was obtained from Assay Designs. 7-Nitro-2,1,3-benzoxadiazol-4-yl (NBD)-labeled α-Toc was kindly provided by J. Atkinson (Brock University, Canada). Bromoenol lactone and methylarachidonyl fluorophosphates were purchased from Cayman Chemicals. The orange fluorescent protein-tagged leader sequence of E1α pyruvate dehydrogenase (Organelle Light), MitoTracker Red CM-H2Ros, and MitoSOX Red were purchased from Invitrogen and used to stain with the mitochondria. The high purity of α-ESA was purchased from Larodan Fine Chemicals (Sweden). Staurosporine was obtained from Tocris Bioscience. 5(and 6)-Chloromethyl-2′,7′-dichlorodihydrofluorescein diacetate (CM-H2DCF-DA) was purchased from Invitrogen. BESSo-AM was purchased from Wako Pure Chemicals (Japan). α-ESA-Me was prepared by reacting α-ESA with trimethylsilyl-diazomethane in 10% hexane solution (TCI, Japan). Trimethylsilyl-diazomethane was added to the reaction mixture (α-ESA, 20.0 mg in 18 ml methanol) drop-by-drop over 1 h at room temperature to avoid by-products. The reaction mixtures were purified with a C_{18} column. The resulting material was stored in a vial under a nitrogen gas atmosphere at −80 °C or below.

Western Blot Analysis—PC12 cells were cultured at 6×10^5 cells/dish in 10-cm poly-L-lysine-coated dishes in a differentiation condition. After 24 h, the cells were cultured with NGF for another 48 h. α-ESA was then added to the cells to induce apoptosis after inhibitors, U0126 or α-Toc, if needed. The cells were collected after 16 h of α-ESA treatment. Briefly, after the cells were washed with Tris-buffered saline, lysates were prepared using Triton-based lysis buffer containing protease inhibitors and phosphatase inhibitors. Neurotropic factor (NGF) was included in the washing buffer to avoid other types of apoptosis caused by neurotropic factor withdrawal from differentiating cells. A ProteoExtract subcellular proteome extraction kit (Calbiochem) was used for the preparation of the nuclear and cytosolic fractions. The cell lysates and subcellular fraction samples were resolved by SDS-PAGE on 5–20% gradient gels and transferred onto polyvinylidene fluoride membranes (ATTO, Japan). The membranes were incubated with primary Abs at 4 °C overnight and then with alkaline phosphatase-labeled secondary Abs for 1 h at room temperature. The blots were detected by an alkaline phosphatase-conjugated substrate kit (Bio-Rad). For Bcl-2 overexpression and siRNA experiments, a chemiluminescent ECL system was used to

detect the blots. Western blot analyses were performed on data from more than three independent experiments.

Immunofluorescent Staining—PC12 cells on poly-L-lysine-coated glass chamber slides were washed twice with Dulbecco's phosphate-buffered saline containing NGF before the cells were fixed with 4% paraformaldehyde (Wako, Japan) for 30 min and permeabilized with cold 0.2% Triton X-100 for 10 min. After blocking with 2% bovine serum albumin for 1 h, the cells were incubated with primary Abs against Bax, AIF, ERK, or phospho-histone H2AX at 4 °C overnight. The cells were washed and incubated with Alexa 488- or Texas Red-labeled secondary antibodies (Invitrogen) and Hoechst 33342 (Invitrogen) or TUNEL (Roche Diagnostics) at room temperature for 1 h. After washing, the cells were mounted with Prolong gold mounting media (Invitrogen). Fluorescent microscopy was performed using an IX71 microscope (Olympus, Japan), a deconvolution microscope DeltaVision personal DV (Applied Precision), and a Leica confocal microscope TCS-SP5 (Leica Microsystems, Germany). Immunofluorescent staining data were obtained from more than four independent experiments.

Caspase-3/7 Assay—PC12 cells were cultured in 10-cm poly-L-lysine-coated dishes in the differentiation condition. The caspase-3 activity of lysates from PC12 cells treated with ESA was measured with the Apo-ONE homogeneous caspase-3/7 assay kit (Promega) according to the manufacturer's protocol using a fluorescent plate reader (Infinity M, Tecan). Data were obtained from two independent experiments.

DNA Analysis—Genomic DNA was extracted from the cells treated with α-ESA for 30 h using FastPure DNA kit (Takara, Japan), and DNA was analyzed using agarose gel electrophoresis and pulse field gel electrophoresis (CHEF DR-II, Bio-Rad). The conditions for the pulse field gel electrophoresis were as follows: 1% agarose, 6 V/cm, 15 °C, 15 h.

Bcl-2 Transfection—The human *bcl-2* was a kind gift from Y. Tsujimoto (Osaka University, Japan). The *bcl-2* was subcloned into the pcDNA-DEST40 expression vector (Invitrogen). PC12 cells (2×10^6 cells/ml) were transfected with the *bcl-2* by an electroporation method (Amaxa Nucleofector II; Lonza, Switzerland) according to the manufacturer's protocol (program U-029). The same numbers of the transfected cells were seeded to 35-mm dishes in the differentiation condition. Twenty four hours after the transfection, the cells were exposed to α-ESA for an additional 24 h. The cell viability was then measured using the WST-8 reagent, and Western blot analysis was performed to check Bcl-2 protein expression. Blots were detected using ECL plus (GE Healthcare) and Hyperfilm (GE Healthcare) following horseradish peroxidase-labeled secondary Abs.

RNA Interference—The knockdown of PARP-1 was performed in PC12 cells using predesigned ON-TARGET*plus* siRNA SMART pool purchased from Dharmacon. The transfection efficiencies were optimized using siRNA optimization kit (Amaxa). The transfections were performed by the electroporation method (Amaxa, program U029), and the same numbers of the transfected cells were seeded to 35-mm dishes. After 24 h of incubation in the differentiation condition, the cells were exposed to α-ESA or MNNG (500 μM, 15 min) for an additional 24 h. ON-TARGET*plus* nontargeting siRNA pool (300 nM) was used as a control for nonsequence-specific effects. The knockdown of MEK1/2 was performed using predesigned Stealth Select siRNA (1 μM) purchased from Invitrogen. Two mixed primers for each target (MEK1 or MEK2) were used for the experiments. Map2k1-RSS301293 and -RSS301295 are for MEK1. Map2k2-RSS339849 and -RSS339850 are for MEK2 (Invitrogen). Stealth RNA interference negative control was used as a control for nonsequence-specific effects. The cell viability was then measured using the WST-8 reagent, and Western blot analysis was performed to check protein expression. The blots were detected using ECL Plus (GE Healthcare) or an alkaline phosphatase-conjugated substrate kit (Bio-Rad).

Microinjection of AIF Antibody—AIF antibody (100 μg/ml, mouse IgG2b) or MOPC21 (100 μg/ml, isotype control for IgG2b) was microinjected into the differentiated PC12 cells using Stamporation apparatus SU100 (Olympus, Japan) and StampoNeedle (ST-ME330CN-20A, Olympus) (25) in 35-mm poly-L-lysine-coated culture dishes. The microinjected cells were exposed to α-ESA (2 μg/ml) after a 6-h incubation. After 16 h of treatment with α-ESA, the cells were stained with propidium iodide.

Bax Localization—The differentiated PC12 cells were treated with staurosporine (STS, 500 nM) or α-ESA (2 μg/ml). The cells were fixed and stained with Bax and MitoTracker Red CM-H2XRos (1 μM).

Measurements of ROS and Potential—Intracellular ROS and mitochondrial superoxides were measured using H2DCF-DA (10 μM) and MitoSOX Red (5 μM), respectively. Differentiated PC12 cells were incubated with CM-H2DCF-DA or MitoSOX for 1 h or 10 min, respectively. After washing, α-ESA was added to the cells. After 2, 5, and 20 h of incubation, the cells were counted to calculate the percentages of ROS-positive cells from a total of 100 cells. Cells that have fluorescent intensities more than the signal to noise ratio of >5 were determined to be positive. ImageJ (version 1.41) software was used to analyze the intensities of the cells. Mitochondrial membrane potential was measured using JC-1 (5 μM).

Statistical Analysis—All data are expressed as the mean ± S.D. The statistical significance was evaluated by one-way analysis of variance followed by the Dunnett's test to compare the data from multiple groups against a common control group (SigmaPlot). Student's *t* test was used to compare the data from two groups. Statistical significance was determined at $p < 0.05$ (indicated with an *asterisk* in the figures).

RESULTS

α-ESA Induces Apoptosis in Neuronal Cells—The time course illustration of the experiments using α-ESA (Fig. 1*A*) were shown with the morphological and nuclear changes in Fig. 1*B*. In both proliferating (nondifferentiated) and differentiated cells, apoptotic cell death was initiated. PC12 cells were seeded 18 h before the addition of NGF. NGF induced strong ERK1/2 phosphorylation between 7 min and 1 h, resulting in the differentiation and neurite outgrowth. Forty eight hours after the addition of NGF, the phosphorylation of ERK1/2 decreased to the basal level. Then α-ESA (2 μg/ml) was added to the differentiated PC12 cells (Fig. 1*C*). α-ESA induced apoptotic cell death in a dose-dependent manner in neuronal PC12, SH-SY5Y, and NG108-15 cells (Fig. 1*D*). The α-ESA-mediated

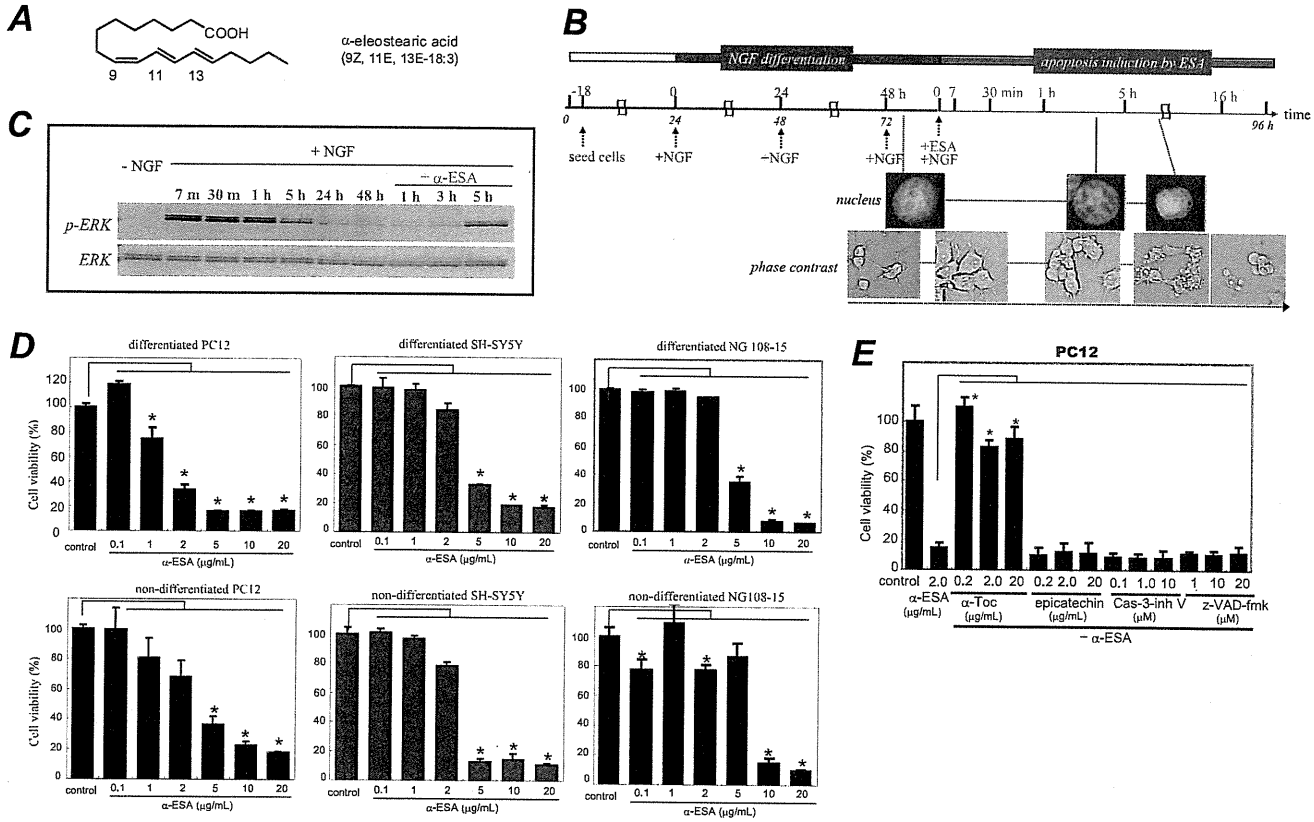

FIGURE 1. **α-ESA induces apoptotic cell death in neuronal cells.** *A*, structure of α-ESA. *B*, time course of α-ESA-mediated cell death in the differentiated PC12 cells. The cells were differentiated by NGF for 48 h and then exposed to α-ESA. *C*, time course of phosphorylation of ERK1/2 during NGF and α-ESA treatment. NGF induced a strong phosphorylation of ERK1/2, and its phosphorylation decreased to the basal level by 48 h. Then the addition of α-ESA induced prolonged and moderate phosphorylation of ERK1/2 again, resulting in the cell death. *D*, α-ESA (2 μg/ml) induced apoptotic cell death in neuronal PC12, SH-SY5Y, and NG108-15 cells. $n = 9$; $p < 0.05$ *versus* control (DMSO alone). *E*, α-ESA-mediated apoptosis was not inhibited by pan-caspase inhibitor Z-VAD-fmk and caspase-3 inhibitor in PC12 cells. α-Toc, but not epicatechin, inhibited the cell death. The values represent the means ± S.D. The viability of α-ESA treated cells was measured by WST-8 reagent 16 h after the treatment. *, $p < 0.05$.

cell death was not inhibited by the pan-caspase inhibitor Z-VAD-fmk and caspase-3 inhibitor V (Z-D(OMe)QM-D(OMe)-fmk) (Fig. 1*E*). Methyl ester of α-ESA did not induce cell death (supplemental Fig. S1).

Effects of MAPK Inhibitors and Antioxidants on α-ESA-mediated Cell Death—A variety of inhibitors was tested to clarify the mechanisms by which α-ESA provoked apoptotic cell death (Fig. 2 and supplemental Fig. S1). The MEK1/2 inhibitor U0126, which inhibits MEK1/2 activity and thereby blocks ERK1/2 phosphorylation, completely abrogated the α-ESA-mediated cell death at a concentration of 5 μM in both nondifferentiated and differentiated cells (Fig. 2*A*). The suppression of phosphorylated ERK1/2 may be important. The cell death was not inhibited by the c-Jun N-terminal kinase (JNK) inhibitor SP600125 and the p38 inhibitor SB203580 (Fig. 2*B*).

Next, the effect of antioxidants on the α-ESA-mediated cell death was examined. Cell death was fully abrogated by α-Toc in neuronal PC12 cells (Fig. 2*C*) but was not inhibited by the green tea antioxidant epicatechin (Fig. 1*E*). Other antioxidants, such as flavonoids (including quercetin and luteolin) and β-carotene, did not reduce the α-ESA-mediated cell death.[3] A trace amount (0.01 μg/ml; equivalent to 23 nM) of α-Toc significantly blocked the cell death induced by 2 μg/ml (equivalent to 7.2 μM) α-ESA (Fig. 2*C*). The inhibitory effects of U0126 and α-Toc on the α-ESA-mediated cell death were also observed in SH-SY5Y and NG108-15 cells (Fig. 2*D*). These results suggest that the α-ESA-mediated cell death is not dependent on neurotropic factors such as NGF, retinoic acid, or dibutyryl-cAMP. Thus, ERK1/2 and α-Toc appear to be a key molecule in the α-ESA-mediated apoptotic cell death.

Transient activation of ERK1/2 occurred when PC12 cells were treated with epidermal growth factor, and sustained activation of ERK1/2 occurred when the cells were treated with NGF (26, 27). After NGF stimulation for a few hours, the sustained ERK1/2 phosphorylation decreased to the basal level in our experiments (Fig. 1*C*). α-ESA was then added to the culture media containing NGF, and the ERK1/2 phosphorylation was investigated at variable intervals in PC12 cells (Fig. 3). Similar experiments were performed in the cells that were pretreated with the MEK1/2 inhibitor U0126 or α-Toc for 30 min. Prolonged ERK1/2 phosphorylation that lasted for at least 16 h was observed in the α-ESA-treated PC12 cells as well as in the camptothecin (CPT)-treated cells. ERK1/2 phosphorylation was observed 2–6 h after the addition of α-ESA and strongly increased by 16 h. U0126 blocked the ERK1/2 phosphorylation

[3] K. Kondo, S. Obitsu, S. Ohta, K. Matsunami, H. Otsuka, and R. Teshima, unpublished data.

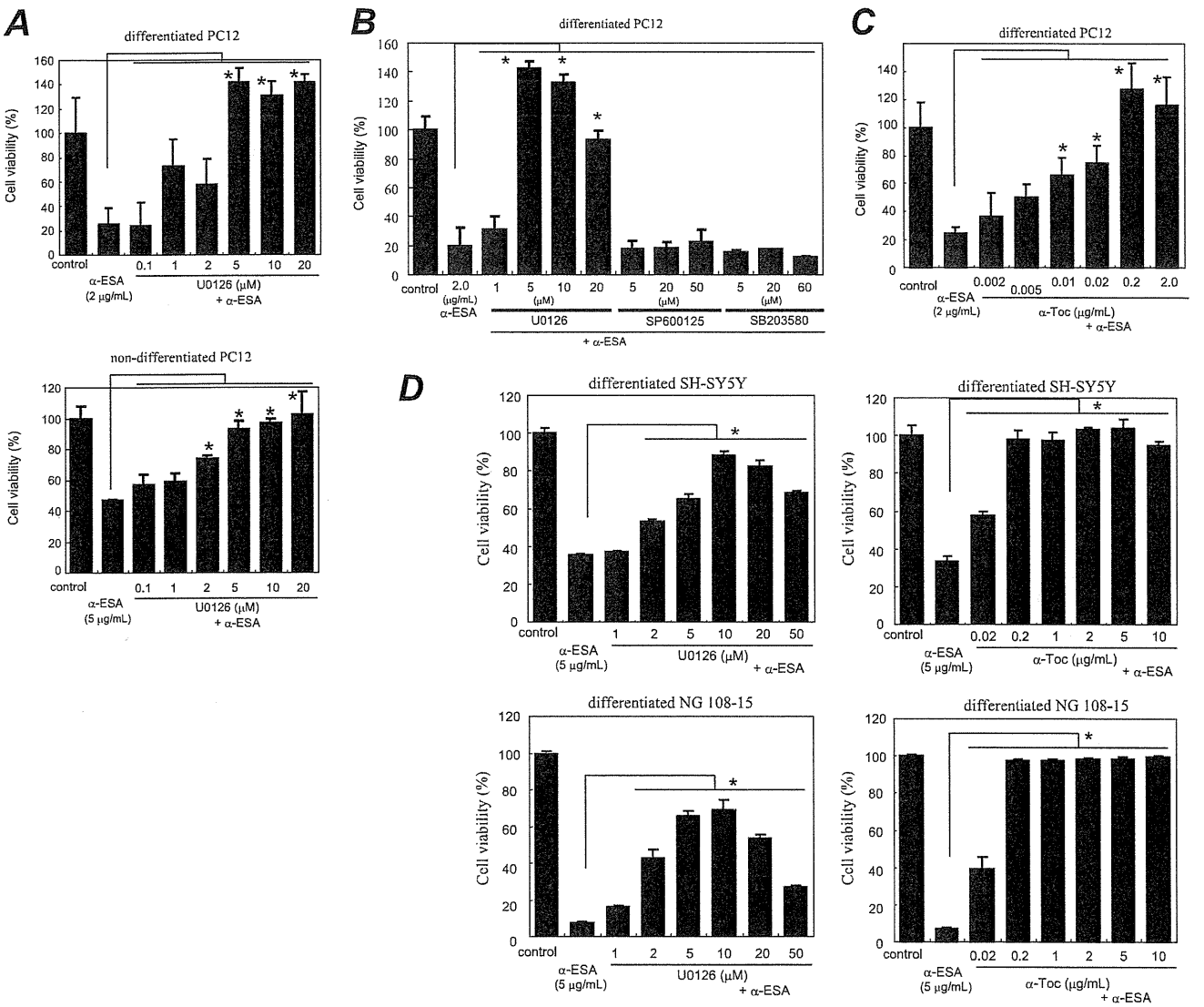

FIGURE 2. **MEK inhibitor and α-tocopherol block α-ESA-mediated cell death.** *A*, MEK inhibitor U0126 prevented α-ESA-mediated cell death in both differentiated and nondifferentiated PC12 cells (5 or 2 μM). $n = 6$; *, $p < 0.05$ *versus* α-ESA alone. *B*, JNK inhibitor SP600125 and p38 inhibitor SB203580 did not block α-ESA-mediated cell death. *C*, α-Toc blocked α-ESA-mediated cell death at lower concentrations (0.01 μg/ml). $n = 6$; *, $p < 0.05$ *versus* α-ESA alone. *D*, in both SH-SY5Y and NG108-15 cells, α-ESA-mediated cell death was blocked by U0126 and α-Toc. The values represent the means ± S.D. The viability of α-ESA treated cells was measured by WST-8 16 h after the treatment.

and thereby prevented the α-ESA-mediated cell death. In contrast, the ERK1/2 phosphorylation was not inhibited by α-Toc, although it completely prevented the cell death (Fig. 3, *A* and *D*). U0126 did not prevent the CPT-initiated apoptosis.[3] These results suggest that the inhibitory mechanism of α-Toc differs from that of U0126.

Next, we examined the activation of caspase-3 during the α-ESA-mediated apoptosis. Caspase-3 was not cleaved to yield an active fragment by α-ESA stimulation over a 16-h time course (Fig. 3*A*). The enzyme activity of caspase-3 was also measured using the fluorescent substrate bis-(*N*-benzyloxycarbonyl-L-aspartyl-L-glutamyl-L-valyl-aspartic acid amide)-rhodamine 110 (Z-DEVD-rhodamine 110). The activity of caspase-3 markedly increased in the CPT-treated cells, whereas no increase in the caspase-3 activity was observed in the α-ESA-treated cells (Fig. 3*B*). CPT was used as a positive control of caspase-3 activation.

ERK1/2 translocation to the nucleus was investigated using confocal microscopy. ERK1/2 migrated to the nucleus 4 h after the induction of apoptotic cell death by α-ESA (Fig. 3*C*). *YZ* planar images confirmed that ERK1/2 was localized in the nucleus. This result was consistent with Western blot analysis data. Actin rearrangement was abrogated in PC12 cells treated with α-ESA. The growth cone of neurite of the cells was significantly suppressed, showing the retardation of pseudopods.

AIF Translocation to the Nucleus and Chromatin Condensation—We next investigated AIF migration upon α-ESA treatment. ERK1/2 was localized in the nucleus when PC12 cells were treated with α-ESA as described above. AIF was initially localized in the mitochondria and migrated to the

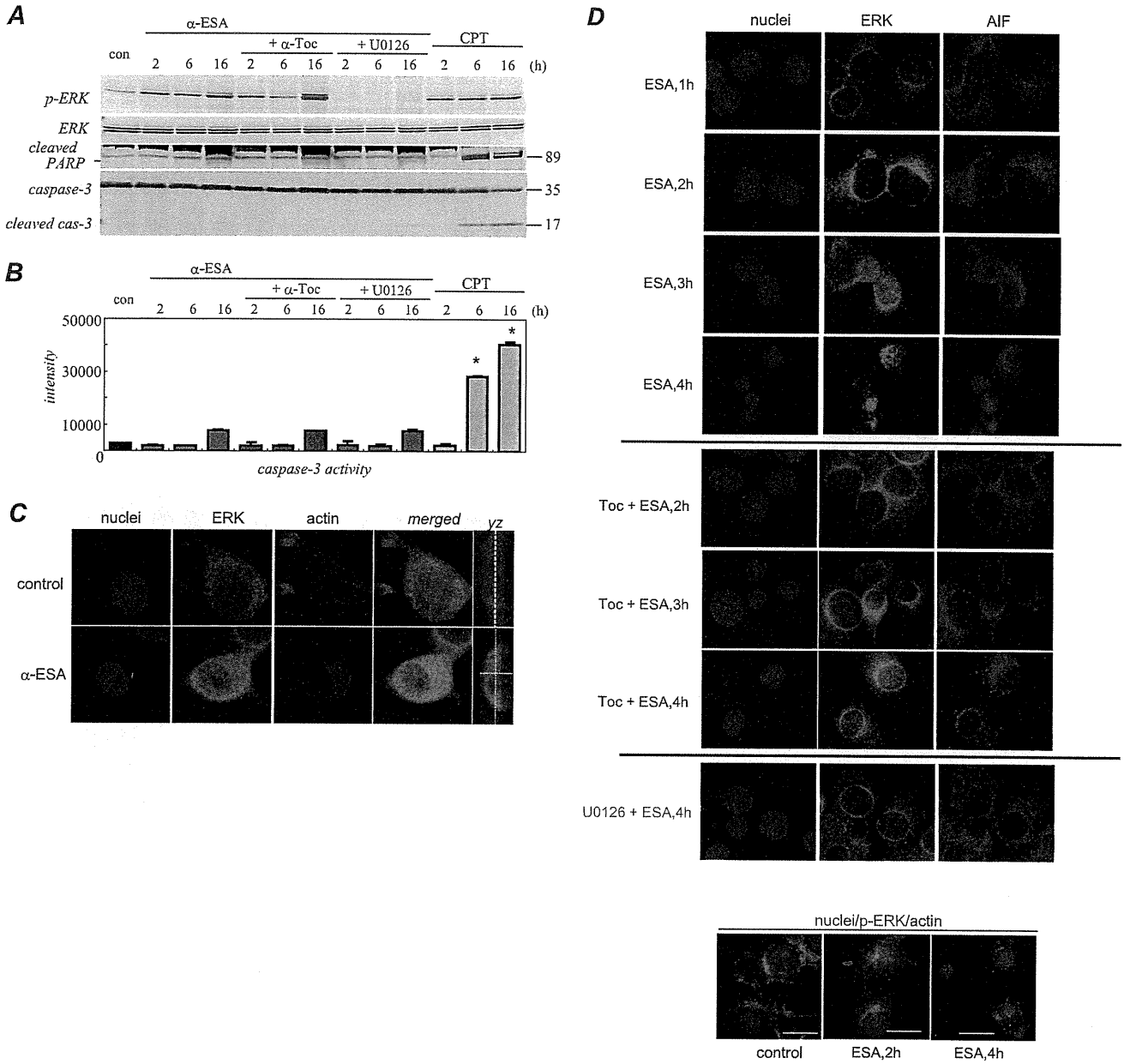

FIGURE 3. **ERK1/2 phosphorylation, PARP-1, and caspase-3 activation induced by α-ESA.** *A*, Western blot samples were prepared from PC12 cells at different time points (2, 6, and 16 h). Western blot analysis was independently repeated three times, and representative data are shown here. ERK1/2 was phosphorylated 2 h or later after α-ESA treatment. U0126 blocked the phosphorylation, whereas α-Toc did not. The cleaved form of PARP-1 (89 kDa) and the active form of caspase-3 (17 kDa) were not detected in α-ESA-treated cells. *con*, control. *B*, caspase-3 enzymatic activity was measured using a fluorescent substrate. The activity remained at the basal level until 6 h after the induction of apoptosis by α-ESA. CPT was used as a positive control of caspase-3 activity. *, $p < 0.05$ *versus* control (DMSO alone). *C*, ERK1/2 migrated to the nucleus upon α-ESA treatment. Images were obtained from samples treated with α-ESA for 4–5 h. Growth cone disappeared, and the actin rearrangements were suppressed. The confocal microscopy images showed that ERK1/2 was localized throughout the nucleus. *D*, treatment of U0126, but not α-Toc, blocked nuclear localization of ERK1/2. The nuclear localization of ERK1/2 and AIF was observed in the α-ESA-mediated cells. Phosphorylated ERK1/2 was observed in the nucleus (*bottom panel*).

nucleus upon α-ESA treatment. At 4 h after the induction of apoptotic cell death, AIF was translocated from the mitochondria to the nucleus, and the number of TUNEL-positive cells was increased. By 7 h after the induction of apoptosis, AIF was mostly localized in the nucleus and DNA compaction occurred (Fig. 4*A*). It was previously reported that when caspase-independent apoptosis was induced, AIF caused the cleavage of DNA into large fragments (~50 kb), which was referred to as stage-I apoptosis (28). Similar DNA cleavage was observed in the α-ESA-treated cells, which was not associated with nucleosomal DNA fragmentation. Pulse field gel electrophoresis revealed the cleavage of DNA into large scale (30–50 kb) fragments in neuronal PC12 cells (Fig. 4*B*). In deconvolution analysis, 30 slices of images were obtained to rebuild three-dimensional images. Data analysis was done using ImageJ software. This result clearly shows AIF localization in the nucleus and the TUNEL-positive nucleus. The subcellular fractions were analyzed by Western blotting. AIF was released from the mito-

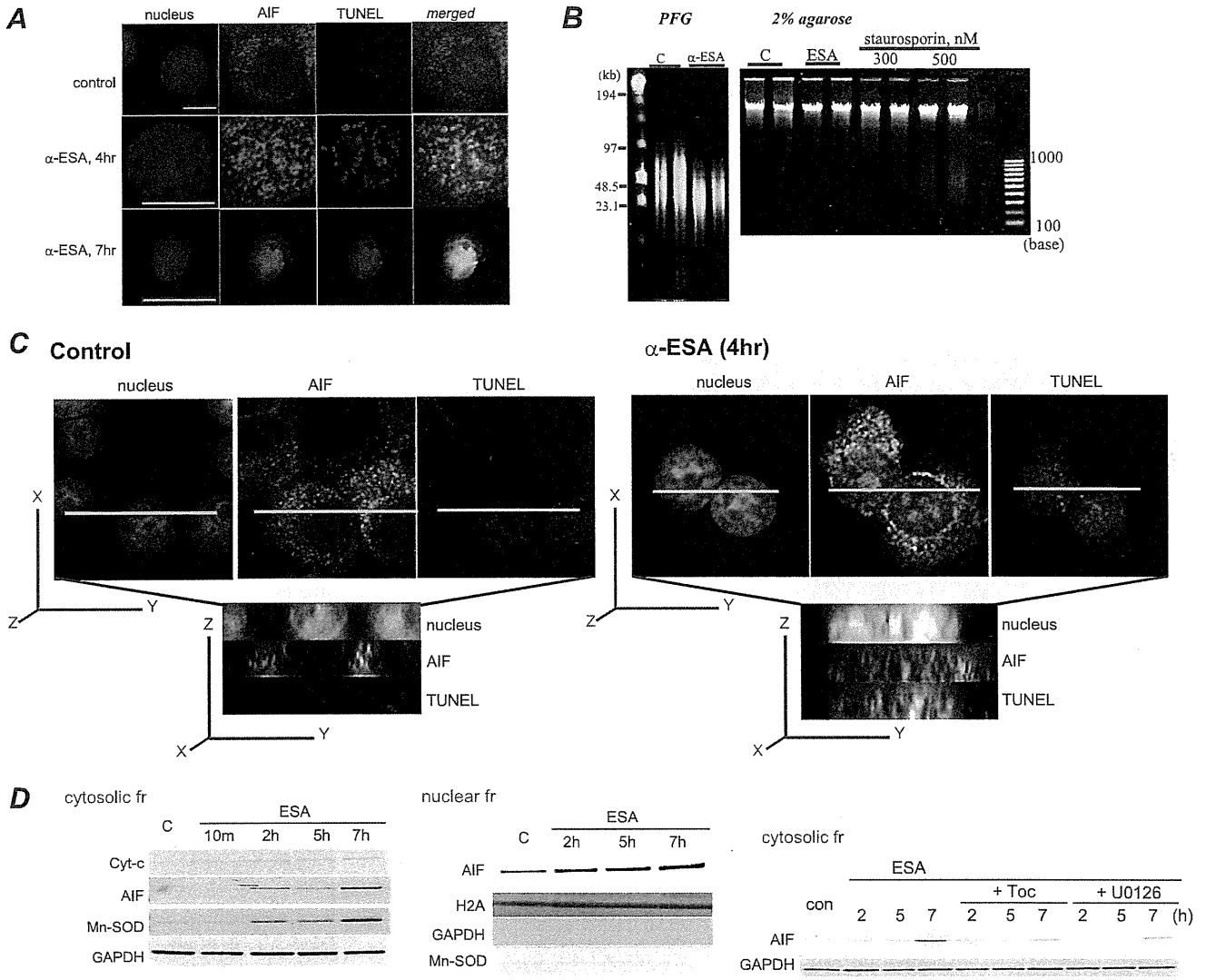

FIGURE 4. **AIF translocation to the nucleus by α-ESA.** *A*, α-ESA induced AIF translocation from the mitochondria to the nucleus. At 4 h after the induction of apoptosis by α-ESA, AIF was translocated to the nucleus (*green*). The nucleus was stained with TUNEL (*red*) and Hoechst (*blue*). *Scale bars* show 10 μm. The TUNEL staining was scattered. By 7 h, the nucleus greatly condensed, and AIF spread throughout the nucleus. The peripheral distribution of chromatin in the α-ESA-treated cell shown was characteristic of AIF-induced stage-I condensation. Images were obtained using the deconvolution microscope. *B*, DNA analysis. Genomic DNA was extracted from PC12 cells that were treated with either DMSO as a control or α-ESA (2 μg/ml) for 30 h. The extracted DNA was analyzed by pulse field gel (*PFG*) electrophoresis. High molecular weight fragments (30–50 kb) were detected on pulse field electrophoresis. Nucleosomal DNA fragmentation was analyzed by 2% agarose gel, showing that α-ESA did not induce nucleosomal DNA degradation. *C*, three-dimensional images of AIF localization in the nucleus. AIF was localized in the whole nucleus, and the nucleus was stained with TUNEL. *D*, subcellular fractionation analysis. The release of AIF and manganese superoxide dismutase (*Mn-SOD*) was observed in the cytosolic fraction (*fr*) of α-ESA-treated cells, resulting in AIF-initiated cell death (*left panel*). The Western blotting of the nuclear fraction revealed AIF localization in the nucleus. There is no contamination of cytosolic and heavy membrane fractions, including mitochondria. α-Toc and U0126 blocked AIF release to the cytosolic fraction (*right panel*). *GAPDH*, glyceraldehyde-3-phosphate dehydrogenase.

chondria into the cytosolic fraction of the α-ESA-treated cells, which was in agreement with the findings of microscopic studies (Fig. 4*A*). In addition, manganese superoxide dismutase was detected in the cytosolic fraction 2–7 h after the induction of the cell death (Fig. 4*D*), suggesting that mitochondrial membrane permeabilization occurred in the α-ESA-treated cells. In addition, the increase in the amount of AIF protein in the nucleus is time-dependent. In this fractionation, there was no contamination from the cytosol or heavy membrane fractions. Finally, the inhibitory effect of α-Toc and U0126 on AIF release was investigated. Both α-Toc and U0126 abrogated AIF release.

PARP-1-independent Cell Death—We next found that the α-ESA-mediated cell death was not abrogated by the PARP-1 inhibitor DPQ at concentrations of up to 100 μM. Moreover, no PAR proteins were detected in Western blot analysis (Fig. 5*A*). This suggests that the α-ESA-mediated apoptotic cell death differs not only from caspase-dependent apoptosis but also from caspase-independent and AIF-mediated apoptosis, which always requires PARP-1 activation, as reported elsewhere (29). To our knowledge, no previous report has described AIF-mediated caspase-independent apoptosis without PARP-1 activation.

DNA damage was also evaluated in the α-ESA-treated cells using anti-phosphorylated histone H2AX (γ-H2AX) Ab. Histone H2AX was phosphorylated in response to DNA damages such as double strand breaks by γ-irradiation. The DNA-alkyl-

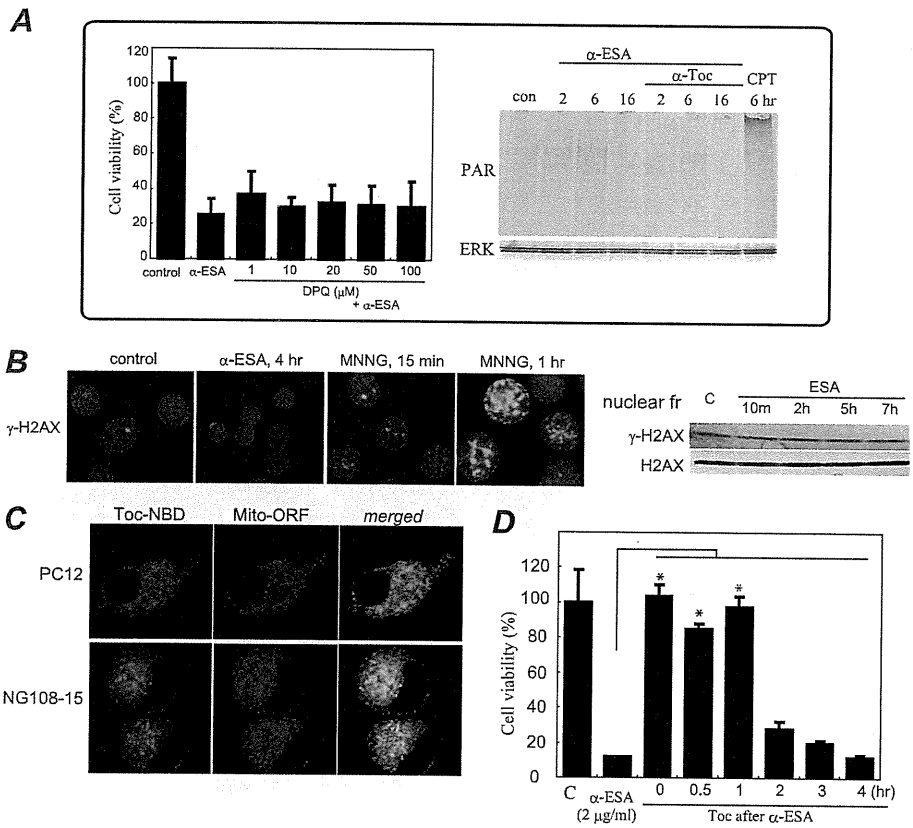

FIGURE 5. *A*, α-ESA-mediated cell death was not inhibited by the established PARP inhibitor DPQ, and PAR proteins were not detected. CPT (40 μM) was used as a positive control for PAR formation. Data were obtained from two independent experiments performed in triplicate (mean ± S.D.). Significance in DPQ-pretreated cells was not observed (*versus* α-ESA alone). *B*, γ-H2AX staining (nuclei in *blue* and γ-H2AX in *green*). Phosphorylation (Ser-139) of histone H2AX (γ-H2AX) was induced by MNNG (500 μM), not by α-ESA (2 μg/ml). γ-H2AX protein levels were not changed in α-ESA-mediated cells. *c*, control. *C*, α-Toc distribution in PC12 and NG108-15 cells was investigated using a confocal microscope. α-Toc is labeled in *green*, and mitochondria are labeled in *red*. The merged images in PC12 and NG108-15 cells show that α-Toc was distributed mostly in the mitochondria. *D*, effect of α-Toc after α-ESA treatment (post-treatment). α-Toc (0.2 μg/ml) was added to the cells at the same time as or after the addition of α-ESA (2 μg/ml). α-Toc blocked cell death 1 h after the addition of α-ESA. Adding α-Toc more than 2 h after α-ESA had no effect. *, $p < 0.05$.

ating agent MNNG induced double strand breaks, whereas α-ESA did not. This indicates that DNA double strand breaks do not arise from the α-ESA-treated cells (Fig. 5*B*).

To clarify the action of α-Toc in these cells, its localization was examined using NBD-labeled α-Toc and orange fluorescent protein-tagged mitochondrial resident protein. In both PC12 and NG108-15 cells, α-Toc mostly migrated to and was localized in the mitochondria (Fig. 5*C*). The localization of α-Toc to the nucleus was not observed in both cell types. The post-treatment with α-Toc 1 h after the addition of α-ESA still blocked the apoptotic cell death (Fig. 5*C*). Recently, ERK1/2 was reported to regulate PARP-1 activation (30, 31). However, PARP-1 itself was not activated in the α-ESA-treated cells.

Microinjection of AIF Antibody—AIF (mouse IgG2b) or MOPC21 (isotype control) antibody was microinjected into the differentiated PC12 cells. The AIF Ab-injected cells blocked the α-ESA-mediated cell death, whereas the MOPC21 Ab-injected cells were killed by α-ESA (Fig. 6*A*). This shows that AIF is a critical factor for the α-ESA-mediated cell death.

Overexpression of Bcl-2—Pro-survival Bcl-2 widely protects apoptosis induced by various stimuli such as camptothecin, etoposide, and staurosporine because Bax/Bak-mediated release of Cyt-c, Smac/Diablo, AIF from mitochondria is blocked by pro-apoptotic Bcl-2 and Bcl-X_L (9, 32, 33). Thus, PC12 cells were transfected with *bcl-2* by the electroporation method (Amaxa Nucleofector II). The amount of Bcl-2 protein in the transfected cells was approximately nine times greater than that in mock-transfected cells according to Western blot analysis. The cell viability was measured using the WST-8 assay reagent for the whole cells. The release of AIF from the mitochondria to the nucleus was suggested to be regulated by Bcl-2 (34). However, the α-ESA-mediated apoptotic cell death was not blocked by Bcl-2 overexpression (Fig. 6*B*). Yu *et al.* (20) reported that Bcl-2 alone was not sufficient to prevent MNNG-treated AIF release and caspase-independent cell death.

RNA Interference of PARP-1 or MEK1/2—α-ESA induced AIF release, resulting in the cell death without PARP-1 activation. The well established PARP-1 inhibitor DPQ did not block the apoptotic cell death. To clarify the involvement of PARP-1 in the α-ESA-mediated cell death, the knockdown experiments for PARP-1 were carried out using siRNA targeted for rat PARP-1. The siRNA-transfected PC12 cells were exposed to α-ESA (2 μg/ml) or MNNG (500 μM) as a positive control in the differentiated condition. The PARP-1 knockdown inhibited the MNNG-treated cell death, whereas the knockdown did not abrogate the α-ESA-mediated cell death (Fig. 6*C*). DPQ treatment of PARP-1 knockdown cells also did not block the cell death (Fig. 6*D*). These results suggest that PARP-1, which is considered to be required for AIF-initiated caspase-independent apoptosis, is not involved in the α-ESA-mediated cell death.

We next investigated whether or not ERK1/2 phosphorylation was critical for the α-ESA-mediated cell death using siRNA targeted for rat MEK1/2. The siRNAs for MEK1 or MEK2 were transfected into PC12 cells, and the cells were exposed to α-ESA (5 μg/ml) in the proliferation condition. The knockdown of either MEK1 or MEK2 effectively blocked the α-ESA-mediated cell death (Fig. 6*E*). Together with the inhibitor (U0126) experiments, these results indicate that ERK1/2 phosphorylation plays an important role in the α-ESA-mediated apoptotic cell death.

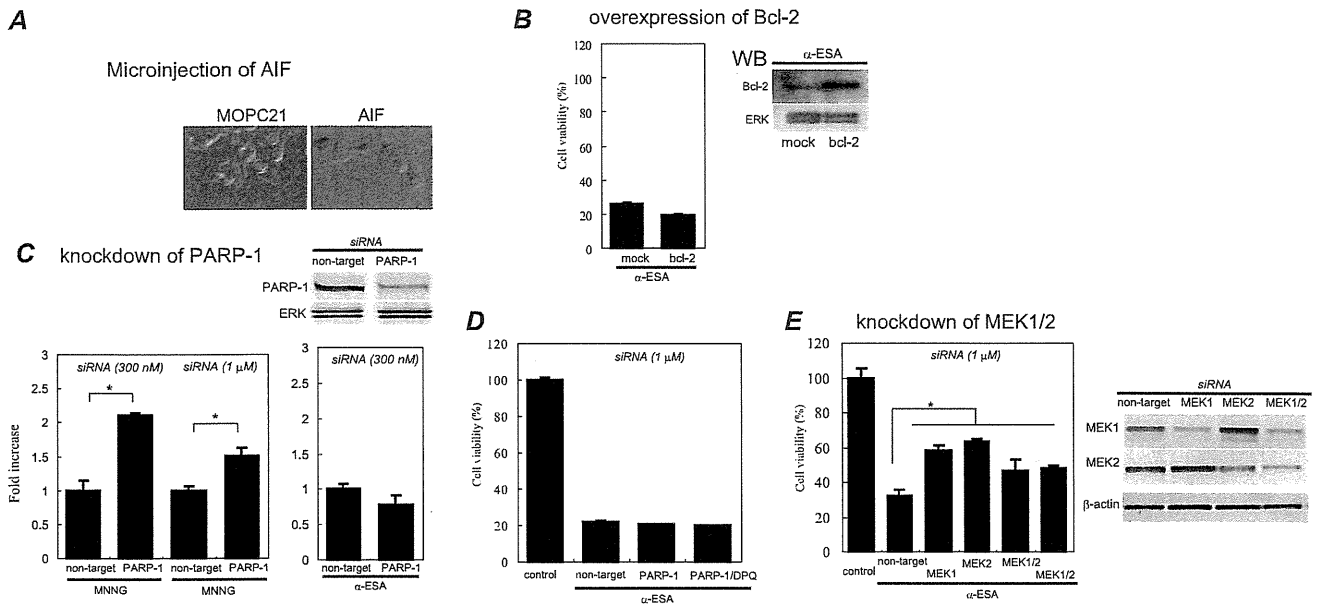

FIGURE 6. **Effect of AIF microinjection, Bcl-2 overexpression, and knockdown of PARP-1 and MEK1/2 on α-ESA-mediated apoptosis.** *A*, microinjection of AIF antibody blocks α-ESA-mediated apoptosis. AIF or MOPC21 (isotype control) antibody (*Ab*) was microinjected into the differentiated PC12 cells using Stamporation apparatus and incubated for 6 h. The cells were exposed to α-ESA (2 μg/ml) for 16 h and stained with propidium iodide. The AIF Ab-microinjected cells blocked α-ESA-mediated cell death, whereas the MOPC21 Ab-microinjected cells did not, stained in *red*, which means the cells were dead. Images were obtained from three independent experiments. All cells in these images were microinjected. *B*, *bcl-2* was transiently transfected into PC12 cells. After 24 h of incubation, the cells were exposed to α-ESA (2 μg/ml) and incubated for another 16 h. The cell viability was measured for the whole cells. The overexpression of Bcl-2 did not protect PC12 cells from α-ESA-mediated apoptosis ($n = 3$). *WB*, Western blot. *C*, siRNA targeted for rat PARP-1 was transfected into PC12 cells. After 24 h of incubation, the cells were exposed to α-ESA (2 μg/ml) or MNNG (500 μM) and incubated for another 16 h. The cell viability was measured for the whole cells. The knockdown of PARP-1 did not block α-ESA-mediated apoptosis, whereas it prevented MNNG-treated (500 μM, 15 min) cells from the apoptosis. ($n = 3$; *, $p < 0.001$). *D*, combination of PARP-1 knockdown and DPQ treatment (50 μM) had no effect on the block of the apoptosis. *E*, siRNA experiments for rat MEK1 and MEK2 were performed in the proliferation condition. The knockdown of either MEK1 or MEK2 significantly blocked α-ESA-mediated cell death ($n = 6$; *, $p < 0.05$). The knockdown of both MEK1 and MEK2 also inhibited the cell death. The transfection efficiency was ~80% judging from the cells transfected with cDNA encoding green fluorescent protein. The blots for the knockdown samples are shown in the *right panel*. The cell viabilities were measured for the whole cells in overexpression and knockdown experiments.

Involvement of Superoxide Anion Radicals and Mitochondrial Membrane Potential in α-ESA-mediated Cell Death—Involvement of ROS in the α-ESA-mediated apoptotic cell death was next investigated using fluorescent probes, CM-5-(and-6)-chloromethyl-2′,7′-dichlorodihydrofluorescein diacetate for total ROS and BESSo-AM (35, 36) and MitoSOX Red for superoxide anion radicals. Intracellular ROS was observed in the α-ESA-treated cells. The ROS production was blocked by α-Toc pretreatment, whereas epicatechin was not able to inhibit ROS production and the apoptotic cell death (Fig. 7*A*). Superoxide anion radicals were produced shortly before the α-ESA-mediated plasma membrane blebbing started (Fig. 7*B*). Some BESSo-positive cells showed normal morphology, and some of the cells started plasma membrane blebbing. The production of superoxide anion radicals was time-dependent. The strongest intensity was observed 5 h after α-ESA treatment. Superoxide anion radicals produced by α-ESA are probably a small quantity because a trace amount of α-Toc (0.01 μg/ml) localized mostly in the mitochondria abrogated the apoptotic cell death. It appears that the α-ESA-mediated cell death is different from that induced by a high concentration of 1-methyl-4-phenylpyridine or 3-nitropropionic acid (>1 mM), which can produce a large amount of ROS and activate caspase. Superoxide production was also measured using MitoSOX Red to detect superoxides in the mitochondria. Superoxide was produced in the α-ESA-treated cells, whereas the cells pretreated with α-Toc scavenged superoxides (Fig. 7*C*). U0126 almost blocked superoxides.

Mitochondrial membrane potential ($\Delta\Phi_m$) was next examined using JC-1 staining. An uncoupler, carbonyl cyanide *p*-chlorophenylhydrazone, in the mitochondria-electron transport chain immediately abrogated the potential. In contrast, the mitochondrial membrane potential gradually decreased over 5 h in the α-ESA-treated cells (Fig. 7*D*). These results suggest that α-ESA initiates a small amount of superoxide anion radicals, thereby inducing the reduction in the mitochondrial membrane potential, which results in the cell death associated with the plasma membrane blebbing.

Bax Localization of α-ESA-mediated Cells—In the STS-treated cells, Bax started to translocate into the mitochondria at 4 h. However, Bax migration to the mitochondria was not observed in the α-ESA-mediated cells (Fig. 8). These results suggest that Bax-induced channel formation in the mitochondrial outer membrane is not involved in the α-ESA-mediated cell death. The data that Cyt-c was not released from the mitochondria into the cytosol before AIF (Fig. 4*D*) support this result.

Putative Cell Death Mechanism Induced by α-ESA—When cells were treated with STS or actinomycin D in the presence of Z-VAD-fmk, caspase activation was blocked. However, Bax and Bak are localized in the mitochondria, resulting in the release of Cyt-c, AIF, and other mitochondrial proteins such as Smac/

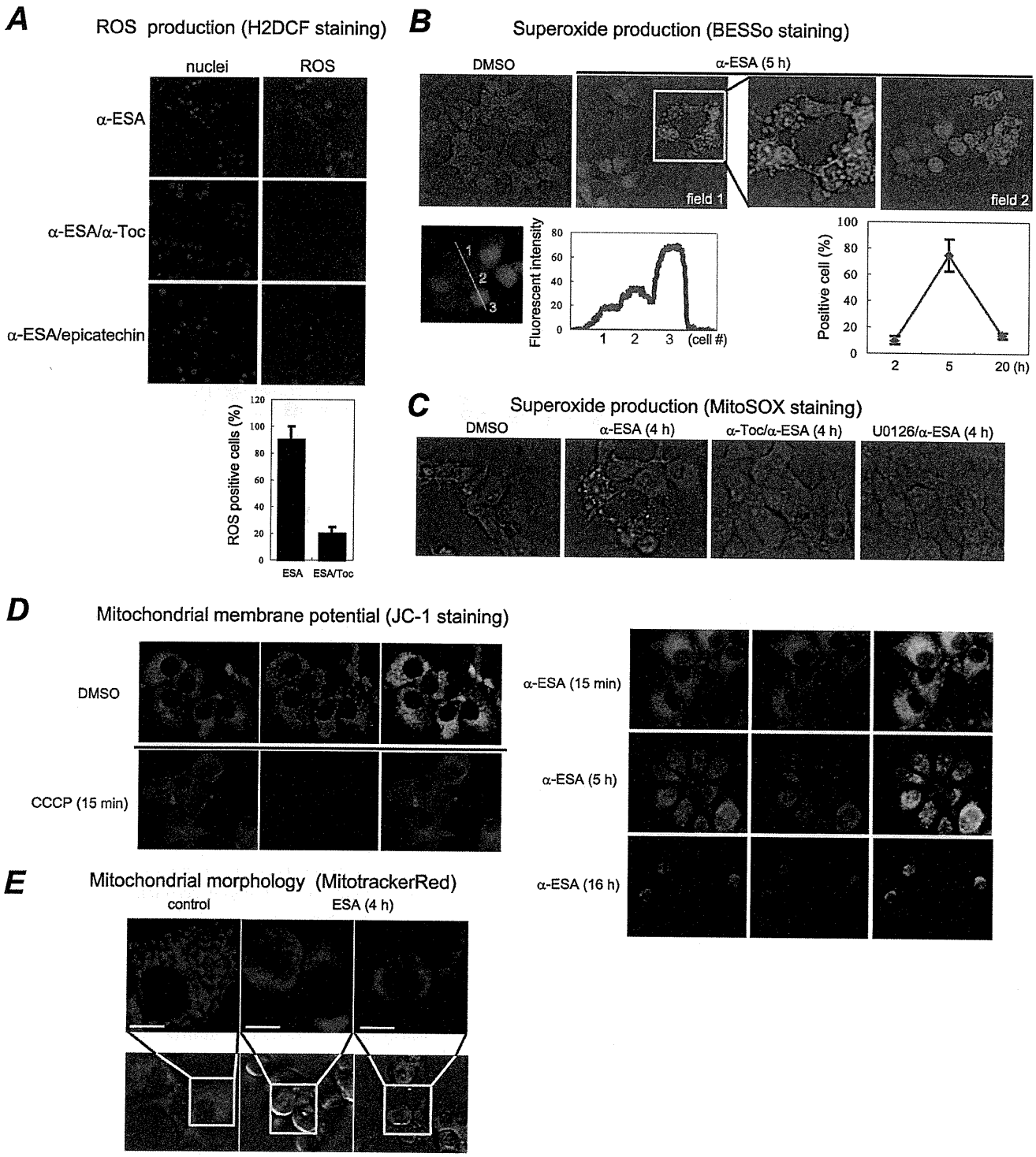

FIGURE 7. **Production of ROS and mitochondrial membrane potential in α-ESA-treated cells.** *A*, intracellular total ROS was measured using H2DCF fluorescent probe. α-ESA initiated ROS, which was blocked by α-Toc (2 μg/ml) but not epicatechin (20 μM). The numbers of ROS-positive cells were counted in the α-ESA-treated cells (12 h) with or without α-Toc. *B*, production of superoxide anion radicals ($O_2^{\cdot-}$) was measured using BESSo fluorescent probe, specific for $O_2^{\cdot-}$. Fluorescent intensities were analyzed by ImageJ software. The cell numbers 2 and 3 that have fluorescent intensities more than the signal to noise ratio of >5 were positive. $O_2^{\cdot-}$ production was observed 5 h after the addition of α-ESA (*bottom right*). Membrane blebbing was observed immediately after superoxide production. *C*, $O_2^{\cdot-}$ was measure by MitoSOX Red indicator. $O_2^{\cdot-}$ was produced in α-ESA-treated cells. α-Toc (2 μg/ml) inhibited the $O_2^{\cdot-}$ production. U0126 (5 μM) almost blocked the $O_2^{\cdot-}$ production. *D*, mitochondrial membrane potential was measured using JC-1. Carbonyl cyanide *p*-chlorophenylhydrazone (*CCCP*) (50 μM) immediately shut down the potential. α-ESA gradually reduced the potential. *E*, mitochondrial morphology during α-ESA-mediated cell death process. Fragmented and condensed mitochondria were observed in the α-ESA-treated cells. *Scale bars* show 8 μm.

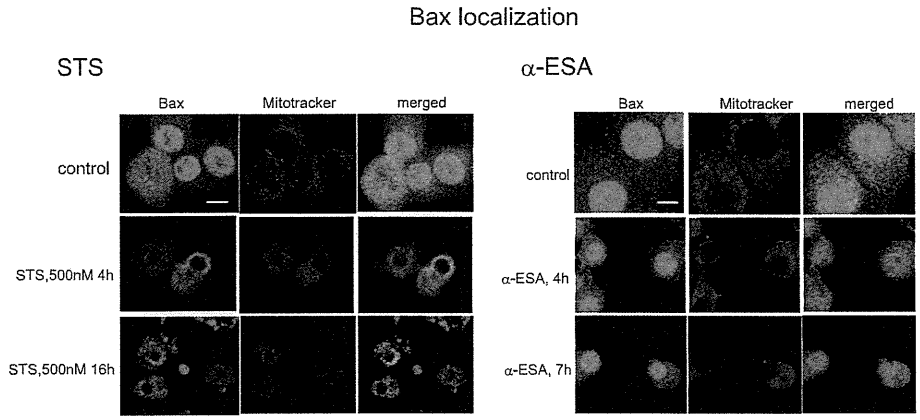

FIGURE 8. **Bax localization of α-ESA-treated cells.** The differentiated PC12 cells were treated with staurosporine (1 μM) or α-ESA (2 μg/ml), and stained with anti-Bax and MitoTracker Red CM-H2Ros. Bax migrated into the mitochondria in the STS-treated cells, whereas Bax did not in the α-ESA-treated cells.

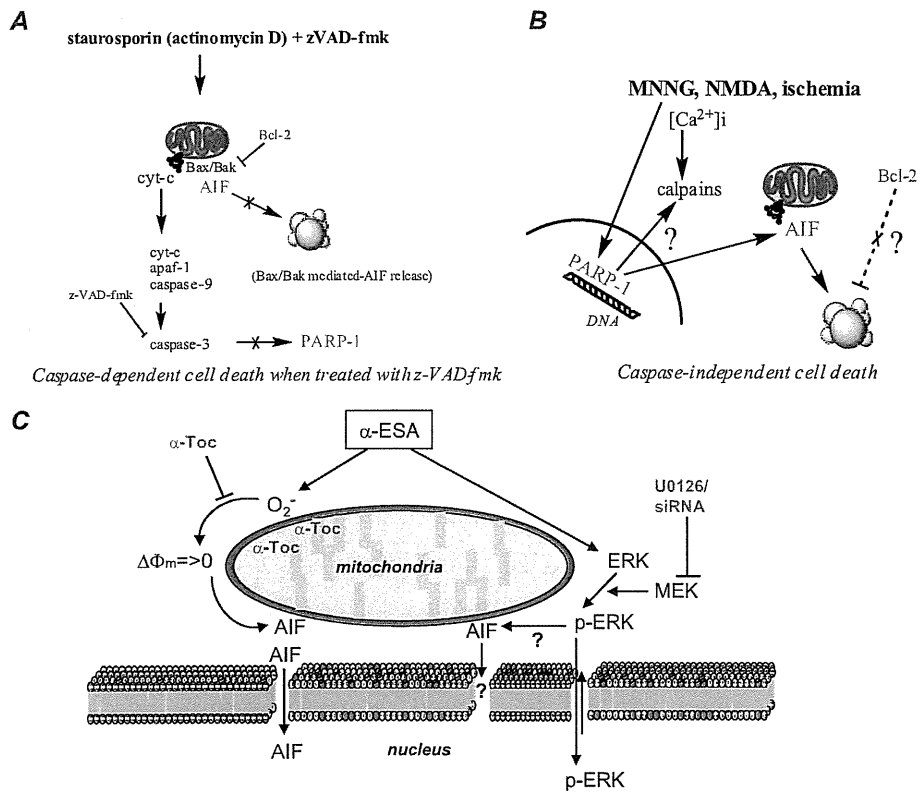

FIGURE 9. **A speculative mechanism of α-ESA-mediated cell death.** *A*, staurosporine + Z-VAD-fmk treatment induces Bax/Bak-mediated Cyt-c, AIF, and other apoptotic mitochondrial proteins such Smac/Diablo, although caspase is blocked by Z-VAD-fmk. This type of apoptosis is blocked by pro-survival Bcl-2 protein. *B*, MNNG, NMDA, or hypoxia ischemia induces the increase in an intracellular Ca^{2+} concentration ($[Ca^{2+}]_i$), intracellular ROS production, and DNA alkylation followed by PARP-1 activation, which results in PARP-1-mediated AIF release, leading to the caspase-independent cell death. *C*, α-ESA induces PARP-1-independent AIF-release, resulting in a novel caspase-independent apoptosis. U0126 and MEK1/2 knockdown block the cell death by unknown mechanisms. ERK1/2 is certainly involved in the cell death. α-Toc blocks ROS production in the mitochondria and cell death without the influence on ERK1/2. PARP-1 is not involved in α-ESA-mediated cell death. α-ESA appears to act separately on MEK1/2-ERK1/2 and superoxide production leading to the reduction of the membrane potential.

Diablo, Omi/HtrA2 (Fig. 9*A*). The excitotoxic NMDA or DNA-alkylating agent MNNG induces DNA damage leading to PARP-1 activation, which results in PARP-1-dependent AIF release and cell death (Fig. 9*B*). In caspase-independent apoptosis, PARP-1 is believed to be a death signal. On the other hand, α-ESA induces PARP-1-independent AIF release through the production of superoxide and ERK1/2 phosphorylation, resulting in caspase-independent and PARP-1-independent cell death (Fig. 9*C*). α-Toc protects the α-ESA-mediated cell death because mitochondrially localized α-Toc can scavenge superoxides. This is a novel and alternative pathway for caspase-independent apoptosis without the involvement of other apoptotic proteins.

DISCUSSION

α-ESA is a conjugated trienoic fatty acid and an isomer of nonconjugated linolenic acid. It has been reported to suppress both tumor growth *in vivo* and angiogenesis *in vitro* by inducing caspase-3 via lipid peroxidation at a concentration of 20 μM (23, 24). α-ESA has been shown to be cytotoxic in human tumor cell lines such as DLD-1, HepG2, and A549, although MCF-7 cells lacking caspase-3 were relatively resistant to the α-ESA-mediated apoptosis (22). These reports suggest that a higher concentration of α-ESA can activate caspase-dependent pathways in non-neuronal cells.

First of all, in this study apoptosis induced by α-ESA was not blocked by both the broad spectrum caspase inhibitor Z-VAD-fmk and caspase-3 inhibitor, but it was inhibited by the MEK inhibitor U0126 and the lipophilic antioxidant α-Toc. The α-ESA-mediated apoptosis was abrogated by as little as 23 nM (0.01 μg/ml) of α-Toc. If the peroxidation of α-ESA is involved in the α-ESA-mediated neuronal death, a similar molar concentration of antioxidants should be needed to protect the cells. In addition, intracellular ROS production caused by the peroxidation of α-ESA can deactivate phosphatases by the oxidation in the active center, leading to the increase in ERK1/2 phosphorylation. This phosphorylation can be inhibited by antioxidants. However, α-Toc did not block the increase in ERK1/2 phosphorylation. Even when α-Toc was